© 2018. Published by The Company of Biologists Ltd | Journal of Cell Science (2018) 131, jcs219956. doi:10.1242/jcs.219956

RESEARCH ARTICLE

The AAA ATPase Afg1 preserves mitochondrial fidelity and cellular health by maintaining mitochondrial matrix proteostasis

Edward M. Germany[1], Nataliya Zahayko[1], Mason L. Huebsch[2], Jennifer L. Fox[2,*], Veena Prahlad[3] and Oleh Khalimonchuk[1,4,*]

ABSTRACT

Mitochondrial functions are critical for cellular physiology; therefore, several conserved mechanisms are in place to maintain the functional integrity of mitochondria. However, many of the molecular details and components involved in ensuring mitochondrial fidelity remain obscure. Here, we identify a novel role for the conserved mitochondrial AAA ATPase Afg1 in mediating mitochondrial protein homeostasis during aging and in response to various cellular challenges. *Saccharomyces cerevisiae* cells lacking functional Afg1 are hypersensitive to oxidative insults, unable to tolerate protein misfolding in the matrix compartment and exhibit progressive mitochondrial failure as they age. Loss of the Afg1 ortholog LACE-1 in *Caenorhabditis elegans* is associated with reduced lifespan, impeded oxidative stress tolerance, impaired mitochondrial proteostasis in the motor neuron circuitry and altered behavioral plasticity. Our results indicate that Afg1 is a novel protein quality control factor, which plays an important evolutionarily conserved role in mitochondrial surveillance, and cellular and organismal health.

KEY WORDS: Mitochondria, Yeast, *C. elegans*, Protein homeostasis, LACE-1, Mitochondrial fidelity

INTRODUCTION

Mitochondria are complex organelles that are essential for cellular physiology. Failure to maintain proper mitochondrial function is associated with altered proteostasis, increased oxidative damage, imbalanced ion homeostasis and a decline in ATP production (Karbowski and Neutzner, 2012; Rugarli and Langer, 2012; Wallace, 2013). Post-mitotic cells with high bioenergetic demand, such as neurons, are particularly vulnerable to these challenges and are usually the most affected by disrupted mitochondrial function (Lin and Beal, 2006; Burté et al., 2015; Levytskyy et al., 2016). To avert such deleterious events, mitochondria are equipped with a number of evolutionarily conserved, dedicated factors and mechanisms – known as mitochondrial quality control (MQC) – that assure the fidelity of the organelle (Rugarli and Langer, 2012; Bohovych et al., 2015a). While the importance of MQC is commonly appreciated, the identities and roles of many of its individual components are only beginning to emerge.

[1]Department of Biochemistry, Nebraska Redox Biology Center, University of Nebraska, Lincoln, NE 68588, USA. [2]Department of Chemistry and Biochemistry, College of Charleston, Charleston, SC 29424, USA. [3]Department of Biology, Aging Mind and Brain Initiative, University of Iowa, Iowa City, IA 52242, USA. [4]Fred & Pamela Buffett Cancer Center, University of Nebraska Medical Center, Omaha, NE 68198, USA.

*Authors for correspondence (okhalimonchuk2@unl.edu; foxjl@cofc.edu)

O.K., 0000-0002-3972-8678

Received 2 May 2018; Accepted 1 October 2018

One group of MQC-related molecules includes proteins that belong to the heterogeneous family of ATPases associated with various cellular activities (AAA). AAA enzymes are oligomeric motors that couple ATP hydrolysis to substrate remodeling by mediating the partial or complete translocation of a polypeptide through a central pore of the typically hexameric enzyme (Erzberger and Berger, 2006; Barthelme and Sauer, 2012). In addition to well-studied AAA proteases that combine ATPase and proteolytic domains (Sauer and Baker, 2011; Glynn, 2017), mitochondria harbor several evolutionarily conserved AAA proteins that perform non-proteolytic functions.

The functional roles of these mitochondrial AAA ATPases are diverse; while some have highly specialized roles, others seem to be involved in a broader range of activities. For example, the sole function of AAA protein Bcs1 is to catalyze translocation of the folded, iron-sulfur cluster-loaded subunit Rip1 of respiratory complex III across the inner mitochondrial membrane (IMM) (Wagener et al., 2011). The mitochondrial AAA unfoldase Mcx1/CLPX has recently been shown to mediate pyridoxal phosphate cofactor insertion into the key heme biosynthetic enzyme 5-aminolevulinate synthase (Kardon et al., 2015). This critical role appears to be independent of the cooperative unfolding–degradation function of the CLPXP complex, which comprises CLPX and the mitochondrial CLPP protease, in higher eukaryotes (Kang et al., 2002; Al-Furoukh et al., 2014). In contrast, the mitochondrial outer membrane-associated AAA protein Msp1/ATAD1 appears to perform less-specific surveillance and membrane extraction functions related to a broader class of mistargeted tail-anchored proteins (Okreglak and Walter, 2014; Chen et al., 2014; Wohlever et al., 2017; Weir et al., 2017).

One mitochondrial AAA enzyme that has largely eluded systematic analysis is Afg1 (also known as AFG1L/LACE1 in mammals) (Lee and Wickner, 1992; Abrahams et al., 2002). In yeast and mammalian mitochondria, this conserved AAA ATPase resides in the matrix and exists as a large, presumably homo-oligomeric (Babu et al., 2012), complex tightly associated with the IMM (Khalimonchuk et al., 2007; Cesenkova et al., 2016a). Previous studies have implicated Afg1 in mitochondrial protein homeostasis by showing that Afg1 aids in the degradation of cytochrome *c* oxidase (CcO) subunits in yeast (Khalimonchuk et al., 2007) and mammalian cells (Cesenkova et al., 2016a), and promotes stress-induced translocation of the tumor protein p53 into mammalian mitochondria (Cesenkova et al., 2016b). However, the significance of these observations and the physiological role of this protein remain far from clear. In addition, we recently identified Afg1 as a multi-copy genetic suppressor of temperature-induced growth defects in yeast strains deficient in the MQC proteases m-AAA and Oma1 (Bohovych et al., 2014). Although this finding further suggests the involvement of Afg1 in MQC, the molecular mechanisms through which this ATPase contributes to mitochondrial homeostasis are unknown.

Journal of Cell Science (2018) 131, jcs219956. doi:10.1242/jcs.219956

In the present study, we characterize Afg1 in the yeast model through an extensive array of genetic and functional tests to demonstrate its functional involvement with MQC proteins, its ability to mediate general protein homeostasis in the mitochondrial matrix and its protective role against oxidative damage. Additionally, we extend this investigation to a metazoan system to show that the roundworm *Caenorhabditis elegans* Afg1 ortholog is also required for mitochondrial protein homeostasis: its loss impairs oxidative stress tolerance and shortens chronological lifespan. In addition, loss of the *C. elegans* Afg1 ortholog causes tissue-specific phenotypes, for instance, impairing aspects of neurotransmission but not overtly affecting muscle function. These findings reveal a new role for Afg1 in mitochondrial and cellular physiology, suggesting that this previously obscure, but conserved, AAA protein is highly relevant to human health and may play tissue-specific roles in maintaining mitochondrial homeostasis.

RESULTS

Afg1 improves mitochondrial function of MQC-compromised cells

To better understand the suppressive effect of Afg1 expression that we observed previously (Bohovych et al., 2014), we carefully evaluated the phenotypes associated with combined loss of m-AAA and Oma1 MQC proteases. The yeast m-AAA protease is a heterohexamer composed of Yta10 and Yta12 subunits, and it is unable to form a functional complex in the absence of either subunit (Arlt et al., 1996; Korbel et al., 2004). Therefore, for our analysis we used a double mutant lacking Oma1 and one of the m-AAA subunits (*oma1*Δ *yta10*Δ). The growth defect of these cells at restrictive temperature on glucose-containing medium indicates an impairment of general mitochondrial function. In agreement with our previous report, overexpression of Afg1 in this *oma1*Δ *yta10*Δ mutant permitted moderate glucose growth relative to the vector control (Fig. 1A). To determine which aspects of mitochondrial function are improved by the overexpression of Afg1, we assessed the mitochondrial network of *oma1*Δ *yta10*Δ cells at the restrictive temperature by performing confocal fluorescence microscopy. While wild-type (WT) and *oma1*Δ cells displayed largely normal mitochondrial networks and normal colocalization of the plasmid-borne mitochondrial marker Su9–red fluorescent protein (Su9–RFP) with the mitochondrial fluorescent dye MitoTracker Green (MTG), the colocalization and network morphology were partially compromised in the *yta10*Δ mutant. Strikingly, *oma1*Δ *yta10*Δ cells showed little to no colocalization of Su9–RFP and MTG, with the MTG staining pattern distinctly differing from a typical pattern of mitochondrial staining (Fig. 1B). Since this abnormal staining pattern resembles that of mitochondrial import mutants, such as *tim23-2* (Dekker et al., 1997), we posited that mitochondria of the temperature-shifted *oma1*Δ *yta10*Δ mutant are grossly depolarized.

To test this idea, we performed flow cytometry analysis of cells stained with the membrane potential-specific dye JC-1. A significant percentage of *oma1*Δ cells (18±2%) and *yta10*Δ cells

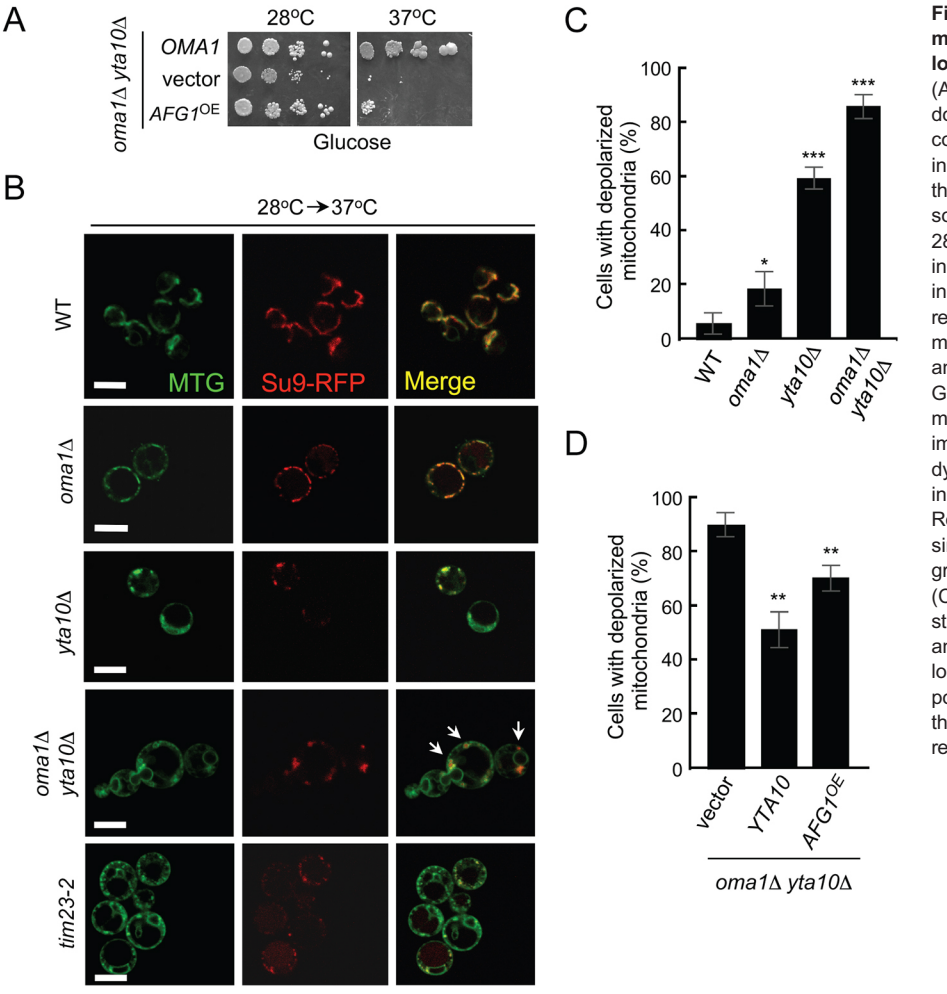

Fig. 1. Afg1 is a genetic suppressor of mitochondrial defects caused by simultaneous loss of the Oma1 and m-AAA proteases. (A) Fermentative growth of the *oma1*Δ *yta10*Δ double mutant transformed with episomal vectors containing *OMA1* or *AFG1*. Cultures were grown in selective SC medium to log phase, normalized through the A_{600}, serially diluted and dropped onto solid SC-glucose medium. Plates were incubated at 28°C or 37°C and photographed after 2 or 4 days of incubation, respectively. (B) Confocal microscopy of indicated strains expressing mitochondria-targeted red fluorescent protein (Su9–RFP) grown in YPD medium for 12 h at 28°C and then subcultured for an additional 6 h at 37°C. The *tim23-2* mutant is a G112E mutation that destabilizes the TIM23 mitochondrial import complex in the IMM and impairs protein import. Cells were stained with the dye MitoTracker Green (MTG). The white arrows indicate aberrant mitochondria-like structures. Representative images are shown consisting of a single focal plane; merged image shows MTG as green and Su9-RFP as red. Scale bars: 5 µm. (C,D) Mitochondrial depolarization in the indicated strains (C) and transformants (D) cultured at 28°C and assessed via flow cytometry analysis of log-phase cells stained with the membrane potential-sensitive dye JC-1. Data are mean±s.d. of three biological replicates, each with n=3 technical replicates; *P<0.05; **P<0.01; ***P<0.001 (t-test).

Journal of Cell Science (2018) 131, jcs219956. doi:10.1242/jcs.219956

(58±4%) contained depolarized mitochondria, and the vast majority (86±5%) of *oma1*Δ *yta10*Δ cells harbored depolarized mitochondria (Fig. 1C), indicating a synergistic effect of the *OMA1* and *YTA10* deletions. Overexpression of *AFG1* (or re-expression of *YTA10*) in the *oma1*Δ *yta10*Δ mutant significantly reduced the percentage of cells with depolarized mitochondria (25±5% and 49±7% reduction for Afg1 and Yta10 expression, respectively; mean±s.d.; Fig. 1D).

To determine whether the observed defects of *oma1*Δ *yta10*Δ cells are associated with impaired proteolysis of proteins that are intrinsic to versus associated with the IMM, we employed a semi-functional m-AAA complex developed by Korbel et al. (2004). This complex contains a Yta10 variant lacking its transmembrane segments (ΔTM), which enables processing of soluble and membrane-associated polypeptides, but not proteins intrinsic to the IMM (Fig. S1). As expected, when WT Yta10, but not its E509Q catalytic mutant form (as a control), was expressed in the *oma1*Δ *yta10*Δ strain, *oma1*Δ *yta10*Δ cells were able to grow on glucose at 37°C. In contrast, expression of the ΔTM form of Yta10 only allowed for marginal proliferation of *oma1*Δ *yta10*Δ cells at 37°C (Fig. S1), suggesting that impaired proteolysis of intrinsic IMM proteins, rather than proteolysis of soluble or membrane-associated proteins, is the cause of the high-temperature growth defect observed for this strain. Taken together, these results suggest that Afg1 may be helping to correct protein homeostasis within the IMM of *oma1*Δ *yta10*Δ cells, thereby reducing mitochondrial depolarization.

Loss of Afg1 function leads to progressive oxidative damage in yeast

We next investigated phenotypes associated with Afg1 depletion. Although *afg1*Δ cells did not exhibit any growth impairment on either fermentable (glucose) or non-fermentable (glycerol/lactate or acetate) medium after 12 h of culture, the respiratory growth of the *afg1*Δ mutant was slightly affected at 5 days of culture as compared to the WT control. Particularly pronounced was the inability of aged Afg1-deficient cells to propagate on acetate medium (Fig. 2A). This result is in agreement with the attenuated levels of several tricarboxylic acid cycle intermediates in *afg1*Δ reported by a previous high-throughput Y3K study (Stefely et al., 2016), and suggests time-dependent impairment of tricarboxylic acid cycle metabolism in the *afg1*Δ mutant. Congruent with an aging-associated mitochondrial deficit, the *afg1*Δ strain displayed a significantly higher percentage of depolarized cells during both exponential and stationary growth phases relative to WT cells (Fig. 2B). *In vivo* analysis of cellular oxygen consumption rates revealed a slight but statistically significant decrease in oxygen consumption rates in 8-day-old *afg1*Δ mutant cells, indicating a mild respiratory deficit (Fig. 2C). This phenotype does not appear to arise from defects in the individual respiratory complexes, as specific enzymatic activities of individual respiratory complexes were largely unaffected by the loss of Afg1 (Fig. S2A). Furthermore, we observed no significant differences in the abundance and distribution of respiratory complexes or their individual subunits in age-matched WT and *afg1*Δ cells (Fig. S2B; note that complex II was undetectable in mitochondrial lysates from both WT and *afg1*Δ cells under exponential growth conditions, likely due to the low abundance of this complex at that growth phase). The nuclear-to-mitochondrial DNA ratios in both exponential and stationary phase *afg1*Δ cells are largely unaltered from WT ratios (Fig. S2C). Moreover, analysis of mitochondrial translational activity, achieved using the *cox1*Δ*::ARG8* reporter strain (Perez-Martinez et al., 2003; Taylor et al., 2017), showed that Arg8 was expressed from the *COX1* locus in *afg1*Δ cells (Fig. S2D, rows 4 and 5 on the SCD −Arg plate).

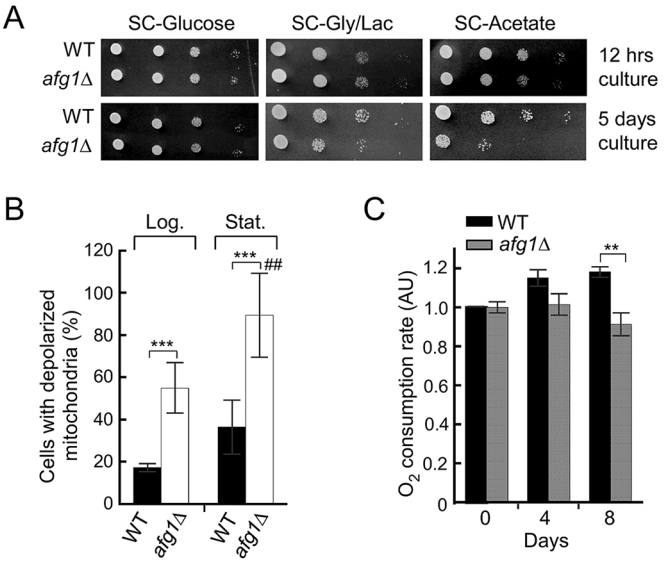

Fig. 2. Loss of Afg1 promotes mitochondrial dysfunction. (A) Growth test of synchronized WT and *afg1*Δ cells grown in SC medium for 0.5 (12 h) or 5 days at 28°C, normalized through the A_{600}, serially diluted, and spotted onto SC plates containing 2% glucose, glycerol/lactate or acetate. Photographs were taken after 2 days (glucose plates) or 4 days (glycerol/lactate and acetate plates). (B) Mitochondrial depolarization in exponential (log; 12 h post-inoculation; A_{600}=0.5; Day 0) and stationary (stat.; 48 h post-inoculation; A_{600}=6.0; Day 3) phase WT and *afg1*Δ cells, determined as in Fig. 1C,D. Data are mean±s.d. (n=3 biological replicates, each with n=3 technical replicates). ***P<0.001 comparing the WT versus the *afg1*Δ strain (*t*-test); ##P<0.01 comparing log-phase *afg1*Δ versus stationary *afg1*Δ cells (one-way ANOVA). (C) Oxygen consumption rates of synchronized WT and *afg1*Δ cells at the indicated day of growth in SC-galactose culture. Data are mean±s.d. (n=4 biological replicates, each with n=3 technical replicates). **P<0.01 (*t*-test).

This result suggests that deletion of *AFG1* in this genetic background did not impair translational activity at the *COX1* locus, regardless of the age of the *afg1*Δ cells.

To gain further insight into the role of Afg1 in mitochondrial physiology, we stained WT and *afg1*Δ cells with the superoxide radical-sensitive dye dihydroethidium (DHE) and quantitatively assessed fluorescence by flow cytometry. Exponentially growing *afg1*Δ cells exhibited an ∼2.2-fold higher DHE fluorescence than WT cells (Fig. 3A), indicating enhanced endogenous superoxide production and implicating superoxide as a likely contributor to the observed phenotype. To validate this finding, we monitored the activity of the mitochondrial enzyme aconitase, which is susceptible to ROS damage owing to its solvent-exposed iron-sulfur cluster (Gardner, et al., 1994), in WT cells and the *afg1*Δ mutant over time. While specific aconitase activity was largely unchanged in the mitochondria of stationary WT cells, we observed a gradual decline in the activity of this enzyme in mitochondria of aged *afg1*Δ cells (Fig. 3B). The steady-state levels of aconitase remained comparable between WT and *afg1*Δ strains under the conditions tested (Fig. S3A). Importantly, the activity of another enzyme with non-surface-exposed iron-sulfur clusters, succinate dehydrogenase, was unaffected in aged *afg1*Δ cells (Fig. S3B), suggesting that the *afg1*Δ defects are not due to perturbations in iron-sulfur cluster metabolism. Consistent with the above data, the activities of mitochondrial superoxide dismutases Sod1 and Sod2 were increased in aged *afg1*Δ cells (Fig. S3C). Finally, we showed that the combined deletion of *AFG1* and *SOD2* results in a synergistic growth defect on medium containing the ROS-generating

Journal of Cell Science (2018) 131, jcs219956. doi:10.1242/jcs.219956

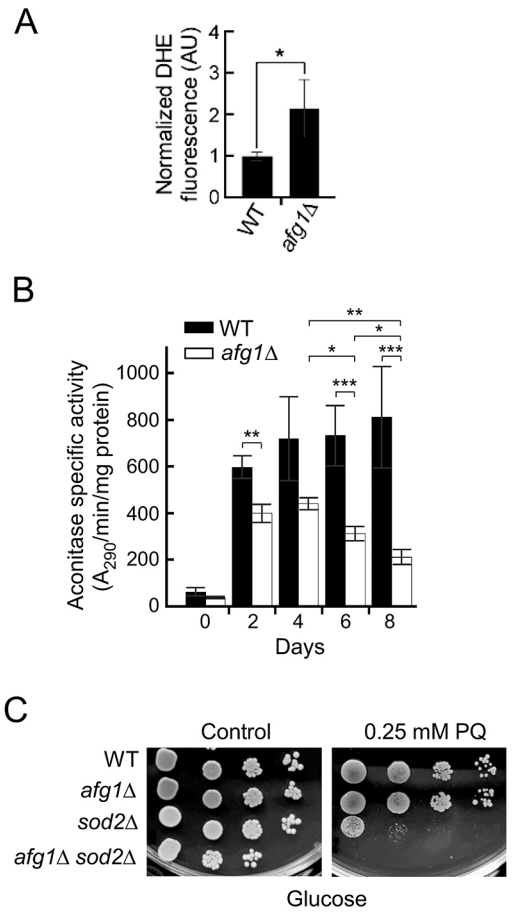

Fig. 3. Cells lacking Afg1 exhibit progressive oxidative damage. (A) Endogenous superoxide levels in WT and *afg1*Δ cells, as assessed by flow cytometry analysis of synchronized log-phase cells stained with the superoxide-specific dye dihydroethidium (DHE). Data are mean±s.d. (n=3 biological replicates, each with n=3 technical replicates). (B) Aconitase specific activity in mitochondria isolated from WT and *afg1*Δ cells that were cultured for the indicated number of days at 28°C. Data are mean±s.d. (n=3 biological replicates, each with n=6 technical replicates). (C) Growth test in the presence of the ROS-generating compound paraquat. The indicated strains were grown to log phase in YPD medium, normalized via the A_{600}, serially diluted, and dropped onto YPD plates with or without 0.25 mM paraquat (PQ). Pictures were taken after 2 days of incubation at 28°C. *P<0.05; **P<0.01; ***P<0.001 (t-test).

compound paraquat (Fig. 3C). These results further support the role of Afg1 in oxidative stress tolerance.

We next interrogated the functional determinants of Afg1 by examining the ability of several structural variants to rescue the oxidative damage phenotype of the *afg1*Δ strain. Since Afg1 is a bona fide member of the AAA family of ATPases (Erzberger and Berger, 2006) within the AAA+ superfamily of P-loop NTPases, some of its key functional residues can be easily deduced from the wealth of structural data available for other AAA enzymes. Taking advantage of this, we engineered three C-terminally 6×His-tagged Afg1 variants impaired in different aspects of ATPase function: (1) an E206Q catalytic mutant unable to hydrolyze ATP; (2) a Y160A pore loop mutant impeded in substrate translocation through the central pore of the enzyme; and (3) a L225D, L226D mutant impaired in its ability to oligomerize. All three variants are expressed (Fig. 4A,B), and gradient centrifugation analysis showed that both the E206Q and Y160A variants are able to form oligomeric complexes of ∼300 kDa, which is consistent with the predicted hexameric architecture of the enzyme (Fig. S4). Expression of each variant was unable to alleviate the aging-associated impairment of aconitase activity in *afg1*Δ cells (Fig. 4A). These data indicate that both the ATP-hydrolyzing and protein-unfolding activities of Afg1, as well as the ability of the enzyme to oligomerize, are critical for oxidative stress tolerance and normal aging in yeast. We were unable to test whether Afg1 directly interacts with aconitase owing to the non-specific binding of aconitase to multiple types of affinity resins that were tested for this purpose.

We also examined genetic interactions between Afg1 and MQC components whose deficiency is associated with intolerance toward oxidative insults, namely the Oma1 (Bohovych et al., 2014) and Pim1/LON (Bota et al., 2002; Bender et al., 2010) proteases. To this end, we generated *afg1*Δ *oma1*Δ and *afg1*Δ *pim1*Δ double deletion mutants and quantitatively tested survival of these strains after acute exposure to 1 mM H_2O_2. In this assay, cells lacking either Afg1, Oma1 or Pim1 exhibited a marked impairment in their ability to form viable colonies following the H_2O_2 challenge (Fig. 4C,D). Importantly, the colony-forming capacity of the peroxide-stressed *afg1*Δ *oma1*Δ and *afg1*Δ *pim1*Δ double deletion strains was further reduced relative to the single deletion mutants, reflecting genetic interaction between *AFG1* and both *OMA1* and *PIM1* (Fig. 4C,D). These results further suggest that Afg1 may function in parallel with key MQC components to promote mitochondrial protein homeostasis.

Afg1 is required for normal protein homeostasis in the mitochondrial matrix

In addition to our data indicating genetic interaction between Afg1 and MQC proteins, Afg1 is similar to well-defined protein quality control AAA proteins (Erzberger and Berger, 2006), and previous reports have suggested a role for this enzyme in facilitating degradation of CcO subunits in yeast and mammalian mitochondria (Khalimonchuk et al., 2007; Cesenkova et al., 2016a). We therefore hypothesized that Afg1 might be working in concert with MQC pathways to maintain mitochondrial protein homeostasis. Since our previous data implicated Afg1 as an IMM-associated resident of the mitochondrial matrix (Khalimonchuk et al., 2007), we focused our attention on protein homeostasis within that sub-compartment. To explore the role of Afg1 in matrix proteostasis, we established two *in vivo* assays for this ATPase. First, we examined the ability of Afg1 overexpression to compensate for inactivation of the key mitochondrial Hsp70 chaperone (Ssc1) by using the *ssc1-2* temperature-sensitive strain (Kang et al., 1990). Cells deficient in this Ssc1 ATPase are impaired in polypeptide translocation through the IMM and protein folding in the matrix (Neupert and Herrmann, 2007), and are also inviable at elevated growth temperature. Re-expression of plasmid-borne Ssc1 permits *ssc1-2* mutant cells to propagate at 37°C on both fermentable and non-fermentable media (Fig. 5A; Fig. S5A). Remarkably, overexpression of Afg1, but not Sco1 (negative control), partially compensates for loss of Ssc1 activity (Fig. 5A; Fig. S5A), indicating that either this AAA enzyme can to some extent fulfill the protein-folding functions of mitochondrial Hsp70 or that Afg1 interacts with Hsp70 to rescue the function of the mutant protein. Moreover, only the WT Afg1, and not its catalytically impaired, substrate translocation-impaired or oligomerization-impaired forms, was able to rescue high-temperature growth of the *ssc1-2* mutant (Fig. 5A), further demonstrating the importance of AAA family biochemical features to Afg1 function.

Secondly, to gain additional insight into the role of Afg1 in matrix proteostasis, we employed a well-established construct

Journal of Cell Science (2018) 131, jcs219956. doi:10.1242/jcs.219956

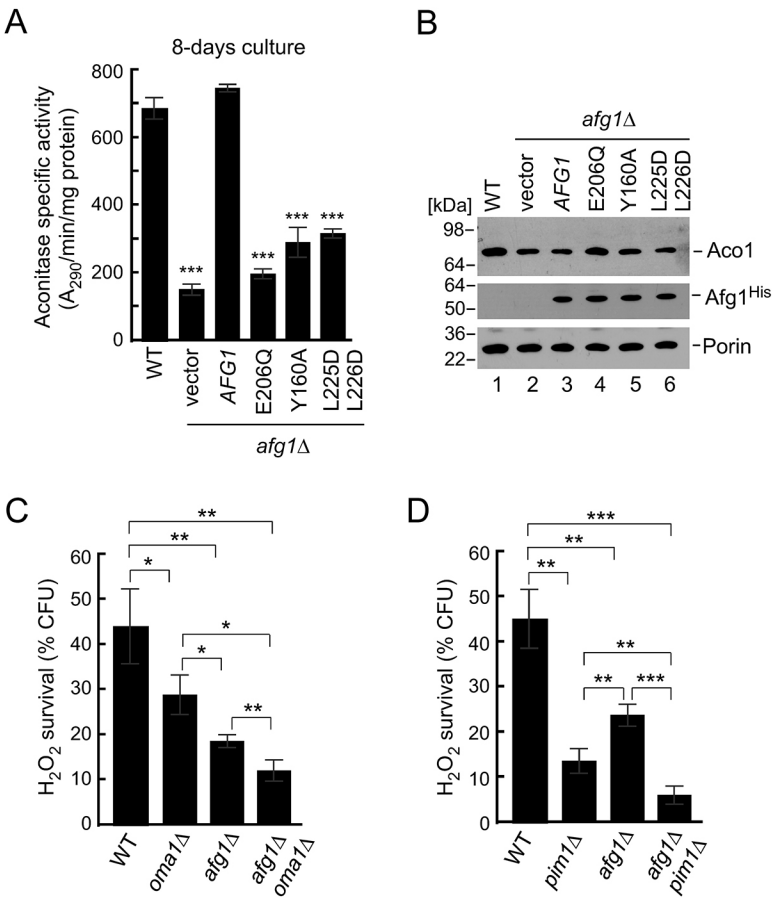

Fig. 4. Afg1 oligomerization and both ATPase and substrate-unfolding activities are required for oxidative stress tolerance during aging, and Afg1 functionally interacts with MQC proteins. (A) Aconitase enzymatic activity in mitochondria isolated from 8-day-old WT and *afg1*Δ cells expressing the indicated Afg1 variants. Data are mean±s.d. (n=5 biological replicates, each with n=3 technical replicates). ***P<0.001 (t-test). (B) Steady-state levels of aconitase (Aco1), 6×His-tagged Afg1 variants and porin in these mitochondria. (C,D) H_2O_2 sensitivity of the indicated strains. Synchronized cells were grown in YPD medium to mid-exponential growth phase at 28°C, normalized via the A_{600}, and acutely stressed with 1 mM H_2O_2 for 1 h at 28°C. Following the incubation, cultures were diluted to 300 cells and plated to test survival on YPD plates. Viable colony-forming units (CFU) were assessed after 2 days of growth. Data are mean±s.d. (n=5 biological replicates, each with n=3 technical replicates). *P<0.05, **P<0.01, ***P<0.001 (one-way ANOVA).

consisting of a misfolding-prone mouse dihydrofolate reductase (mx-DHFRmut) bearing a modified yeast cytochrome b_2 precursor sequence that targets the hybrid protein to the matrix (Fig. 5B; Vestweber and Schatz, 1988; Schreiner et al., 2012). We expressed this mx-DHFRmut construct or its properly folding variant (mx-DHFR) under the control of a galactose-inducible promoter in WT and *afg1*Δ cells (Fig. 5C) and examined the growth of these transformants on glucose (control without induction) and glucose/galactose (induced) media. The presence of mx-DHFR and mx-DHFRmut reduced the fermentative growth of both WT and *afg1*Δ cells. Reproducibly, expression of the mx-DHFRmut variant more severely impaired fermentative growth of the *afg1*Δ strain, relative to WT control (Fig. 5D). Quantitative comparison of the colony-forming capacity of these transformants on glucose/galactose plates confirmed a ∼20% decrease in survival of the *afg1*Δ cells expressing mx-DHFRmut relative to the controls (Fig. 5E). In contrast, we did not observe any differences in the growth of WT and *afg1*Δ strains expressing the intermembrane space (IMS)-targeted version of DHFRmut (Vestweber and Schatz, 1988), as a control (Fig. S5B). These results suggest a role for Afg1 as a MQC factor involved in maintaining protein homeostasis in the mitochondrial matrix. Collectively, our results strongly suggest that Afg1 specifically contributes to mitochondrial matrix proteostasis through its AAA ATPase function.

Afg1 function is evolutionarily conserved

The evolutionary conservation of Afg1 suggests its function may be similar throughout eukaryotes. To test this hypothesis, we examined the function of the roundworm *C. elegans* Afg1 ortholog LACE-1, a product of the gene *C30F12.2*/*lace-1*. We first determined whether *C. elegans* LACE-1 could function in place of yeast Afg1. LACE-1 with a C-terminal 6×His tag cloned from *C. elegans* cDNA into a yeast expression vector was found to be stably expressed, targeted to yeast mitochondria and able to form ∼300 kDa complexes, matching the size of the yeast enzyme (Fig. S6A). Importantly, LACE-1 expression from a yeast episomal plasmid promoted high-temperature growth of the *ssc1-2* yeast mutant (Fig. 6A) and averted oxidative inactivation of aconitase in aged *afg1*Δ yeast cells (Fig. 6B). We conclude that LACE-1 is a bona fide metazoan homolog of Afg1 and that the function of the enzyme is evolutionarily conserved.

Similar to our observations in yeast, we found that aconitase-specific activity was decreased in mitochondria isolated from a *C. elegans c30F12.2(ok3505)* strain in which the gene is disrupted, relative to the N2 WT (Fig. 7A). As with yeast, this decrease occurred only in mitochondria isolated from older (5-day-old animals) but not young adult *c30F12.2(ok3505)* animals. In contrast, there was no significant difference in succinate dehydrogenase activity in mitochondria from aged WT and LACE-1-depleted animals (Fig. S6B). LACE-1-deficient animals were also more susceptible to oxidative stress, as seen with yeast cells; exposure of *c30F12.2(ok3505)* animals to the oxidative stress-inducing respiratory complex I inhibitor rotenone induced a dramatic retardation of growth when compared to wild-type animals (Fig. 7B, C). While the majority of WT animals (84±17%; mean±s.d.) matured to larval stage 4 (L4) or young adults by 4 days after hatching when grown on 5 µM rotenone, the majority of LACE-1-deficient animals (77±9%) remained arrested at larval stages 1, 2 or 3 under the same conditions (Fig. 7B,C). Consistent with the observation that LACE-1 activity was required for protection

Journal of Cell Science (2018) 131, jcs219956. doi:10.1242/jcs.219956

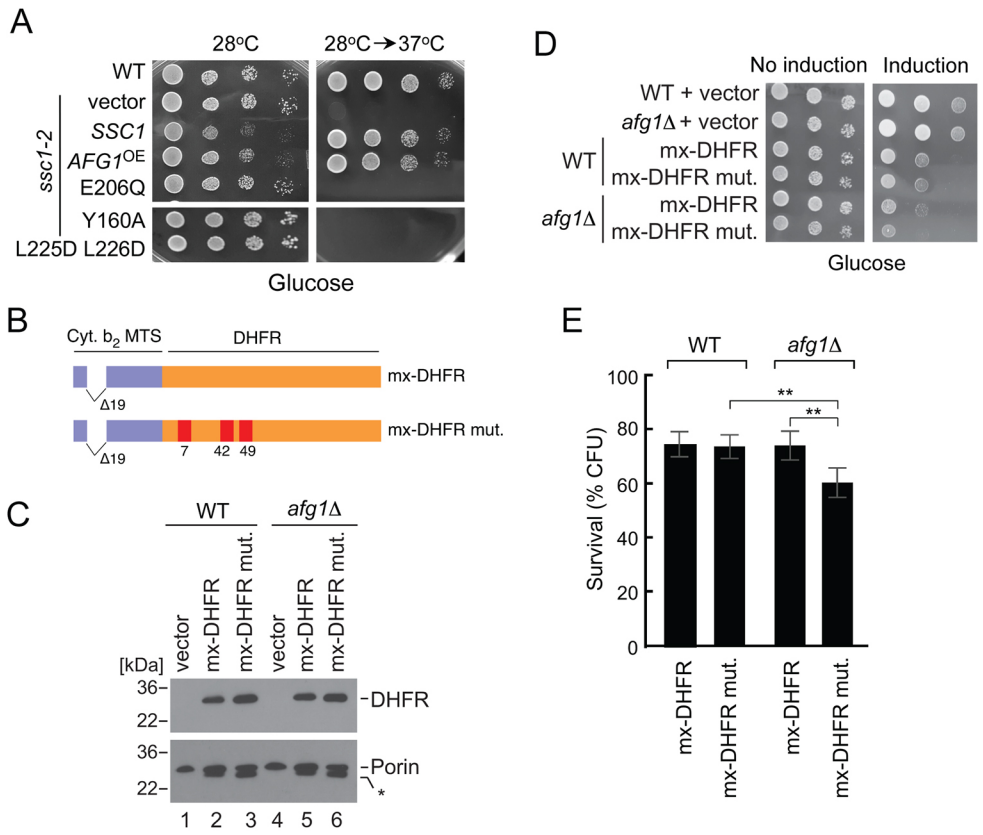

Fig. 5. Afg1 mediates protein homeostasis in the mitochondrial matrix. (A) Fermentative growth of WT and *ssc1-2* cells expressing vector control, *SSC1*, *AFG1* or the indicated Afg1 variants. Cells were handled as described in Fig. 1A. (B) Schematic depiction of dihydrofolate reductase (DHFR) constructs consisting of WT or the misfolding-prone C7A, S42C, N49C variant of mouse DHFR. These matrix DHFR constructs (mx-DHFR and mx-DHFR mut., respectively) are targeted to the matrix compartment by the mitochondrial targeting/sorting moiety of yeast cytochrome b_2 (Cyt. b_2) with a 19-amino-acid deletion that negates IMS sorting. (C) Steady-state protein levels of matrix-targeted normal and mutant DHFR and porin in mitochondria from WT and *afg1*Δ cells. Mitochondria were isolated from mid-exponential growth phase cells cultured in selective medium containing 2% galactose and 0.1% glucose (SC-glucose/galactose) to induce the expression of the DHFR constructs. The asterisk marks a non-specific band. (D) Growth test of WT and *afg1*Δ cells expressing vector control or indicated variants of DHFR. Cells were grown to mid-log phase, normalized via the A_{600}, serially diluted, spotted onto selective SC-glucose (no induction) or SC-glucose/galactose (induction) plates, and cultured for 3 days at 28°C. (E) Colony viability of the indicated WT and *afg1*Δ transformants, cultured as described in D. Cultures were diluted to 300 cells and plated, to assess growth, on SC-glucose/galactose plates. The number of viable colony-forming units (CFU) was assessed after 2 days incubation at 28°C. Propagation efficiency of the respective cells on SC-glucose served as a denominator. Data are mean±s.d. (n=3 biological replicates, each with n=3 technical replicates). $^{**}P$<0.01 (t-test).

against oxidative stress, genetic depletion of LACE-1 using whole-body RNAi knockdown activates a mitochondrial unfolded protein response (UPRmt), as indicated by enhanced expression of UPRmt marker heat-shock protein fluorescent reporters *hsp-6*::GFP and *hsp-6*::GFP, relative to what was seen with control RNAi (Fig. 7D). The upregulation of UPRmt may be a specific response of animals to chronic oxidative stress because *hsp-4*::GFP fluorescence, the endoplasmic reticulum-specific UPR, is not activated (Fig. 7D).

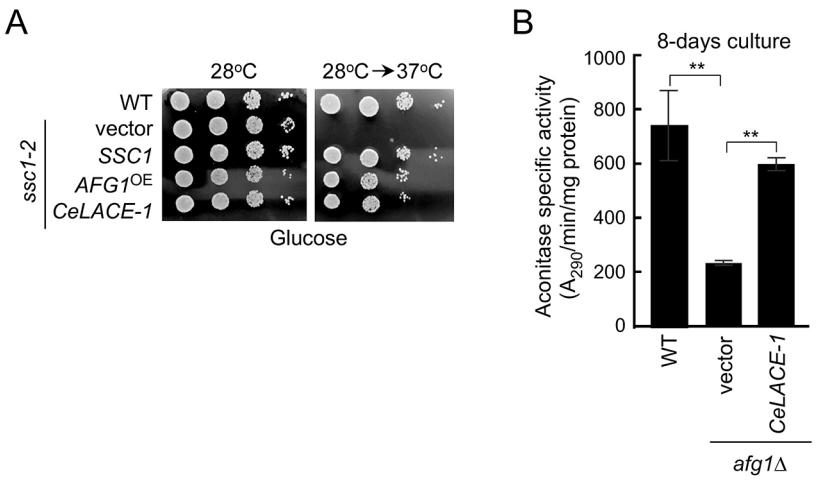

Fig. 6. *C. elegans* ortholog of Afg1, LACE-1, can functionally substitute for the yeast enzyme. (A) Suppression of the high-temperature growth defect of the *ssc1-2* mutant by *C. elegans* LACE-1 (*CeLACE-1*), analyzed as in Fig. 5A. (B) Aconitase enzymatic activity in mitochondria from chronologically aged WT cells and *afg1*Δ cells expressing vector control or *CeLACE-1*, analyzed as in Fig. 4A. Data are mean±s.d. (n=4 biological replicates, each with n=3 technical replicates). $^{**}P$<0.01 (t-test).

Journal of Cell Science (2018) 131, jcs219956. doi:10.1242/jcs.219956

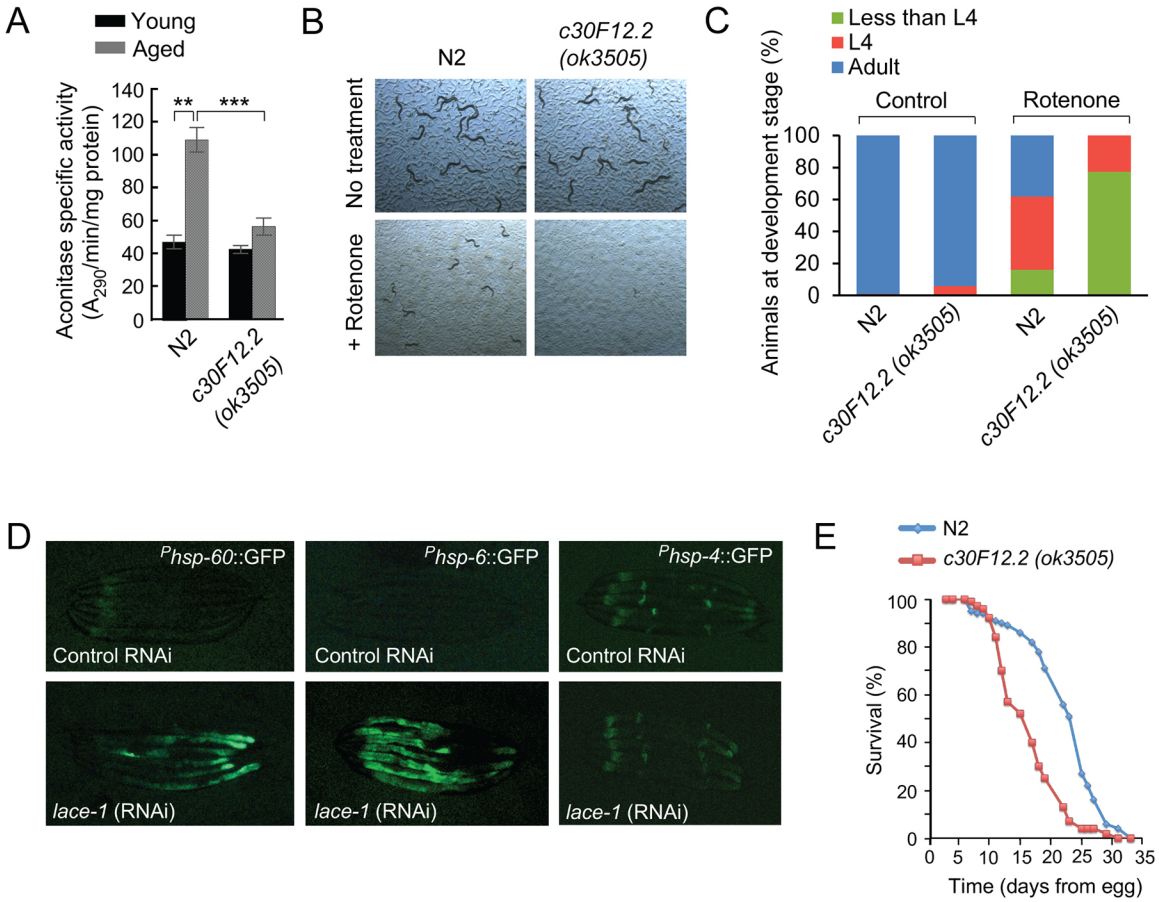

Fig. 7. Worms lacking LACE-1 exhibit shorter lifespan and reduced tolerance to oxidative stress. (A) Enzymatic activity of aconitase in mitochondria isolated from 1-day-old (young) and 5-day-old (aged) N2 and *c30F12.2(ok3505)* worms. Data are mean±s.d. (*n*=3 biological replicates, each with *n*=3 technical replicates). ***P*<0.01; ****P*<0.001 (*t*-test). (B) Representative micrographs of N2 and *c30F12.2(ok3505)* young adult animals that have been exposed to 5 µM rotenone or left untreated. Results are shown for one experiment, representative of three independent replicates. (C) Quantitative analysis of N2 and *c30F12.2(ok3505)* animal development with or without rotenone challenge (*n*=3; 100–150 animals per group per replicate). (D) Fluorescence microscopy images of the mitochondrial unfolded protein response reporters *hsp-60::*GFP and *hsp-6::*GFP and the ER unfolded protein response reporter *hsp-4::*GFP in N2 animals grown on plates containing *E. coli* expressing control vector or *E. coli* with *c30F12.2/lace-1* (RNAi) construct. (E) Lifespan of N2 and *c30F12.2(ok3505)* animals; *n*=5 independent experiments with 10 animals per group.

In *C. elegans*, RNAi inhibition of mitochondrial electron transport chain (ETC) genes can cause a dose- and developmental stage-dependent extension in lifespan via activation of UPRmt. However, activation of UPRmt is not always protective, and knockdown of proteins important for transport of mitochondrial-localized proteins into mitochondria, including *tomm-22* and proteins that function in the TIM23 complex, impair ETC function and activate UPRmt, yet decrease lifespan (Bennett et al., 2014; Bárcena et al., 2018). Therefore, to examine the effects of disruption of LACE-1 on lifespan, we examined the lifespan of *c30F12.2(ok3505)* animals when compared to WT (Fig. 7E). The loss of LACE-1 markedly reduced the lifespan in animals, suggesting that its role in the maintenance of mitochondrial matrix proteostasis, through its AAA ATPase function, impacted more aspects of physiology than simply protecting against oxidative stress.

The loss of Afg1 function causes cell type-specific deficits during normal growth of *C. elegans*

To gain a better understanding of the requirement for LACE-1 in metazoan physiology, we examined whether *c30F12.2(ok3505)* animals show marked phenotypes under normal growth conditions. In *C. elegans*, most treatments that disrupt mitochondrial function have multiple phenotypic effects, such as a retardation of developmental rates, disrupted germline development and fecundity, disruption of body wall muscle cell integrity and neurodegeneration.

Surprisingly, the *c30F12.2(ok3505)* worms did not display gross phenotypic changes as either larvae or adults. For instance, the rates of egg laying in both *c30F12.2(ok3505)* animals and wild-type (N2) animals were similar, and whole *c30F12.2(ok3505)* animals, as examined by DAPI staining, had wild-type germline and oocyte morphology (Fig. S6C). LACE-1-deficient eggs also developed at comparable rates: although *c30F12.2(ok3505)* animals took slightly longer than N2 animals to mature into L4 animals, this increase in developmental timing was not significant (Fig. 7C). Muscle contractions, as measured by pharyngeal pumping rates, were also similar between N2 animals and *c30F12.2(ok3505)* animals (Fig. S6D). LACE-1-deficient worms exhibited normal locomotion (crawling on solid surfaces) compared to N2 control animals, regardless of the age tested (young adults versus 5-day-old animals; Fig. 8A). Consistent with a lack of muscular defects, morphometric assessment of muscle tissues and their mitochondrial network in a ^{P}*myo-3*::mitoGFP reporter strain revealed no significant differences between age-matched controls and *c30F12.2(ok3505)* animals (Fig. S6E).

Journal of Cell Science (2018) 131, jcs219956. doi:10.1242/jcs.219956

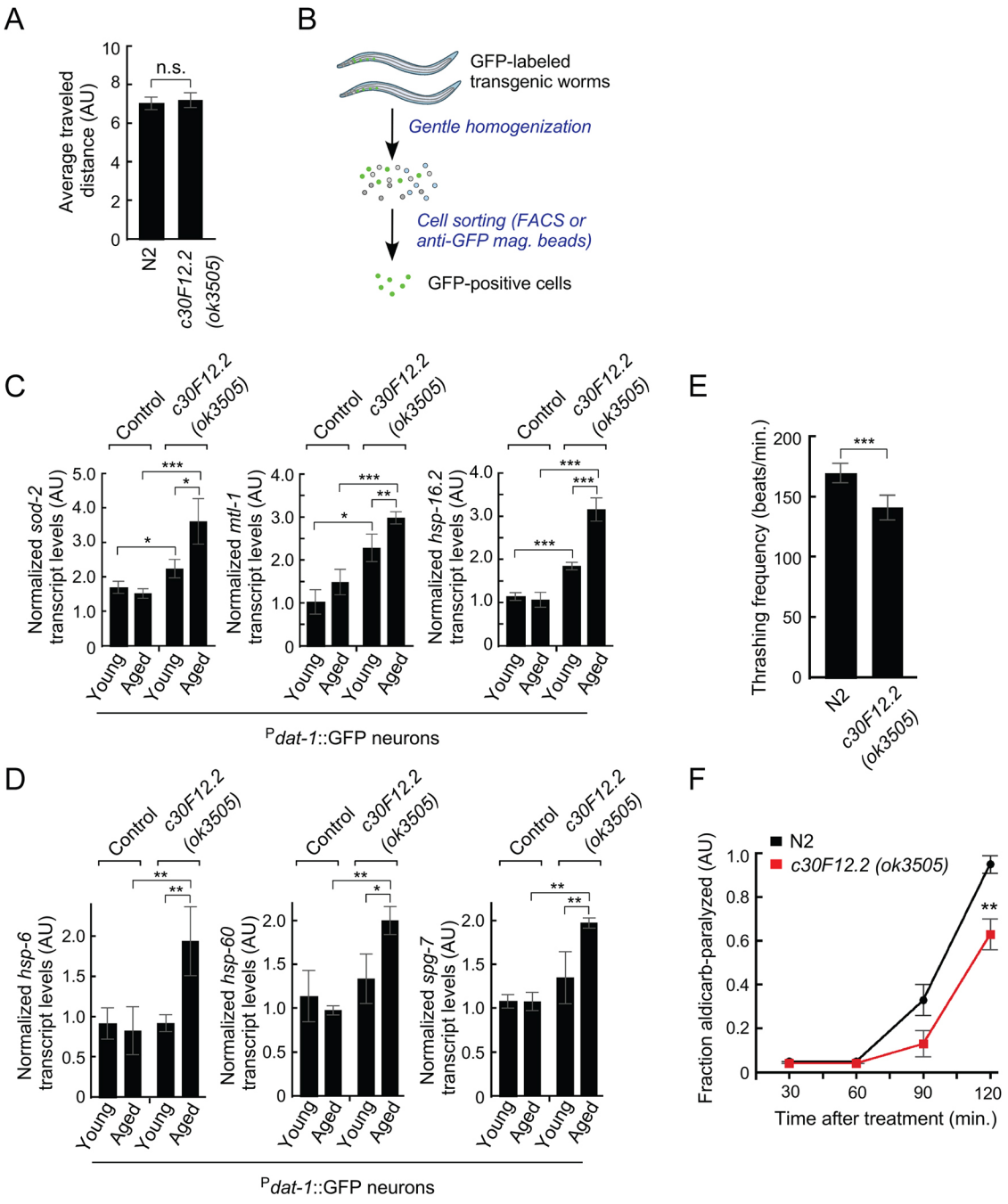

Fig. 8. LACE-1 is required for oxidative stress tolerance and normal mitochondrial protein homeostasis in neurons. (A) Movement of N2 and *c30F12.2(ok3505)* animals on a solid surface at day 1; *n*=3 with 25–30 animals per group. Data are mean±s.d.; n.s., not significant. (B) Schematic workflow depiction for the isolation of specific populations of GFP-labeled cells from *C. elegans* transgenic strains. (C,D) Expression levels of the indicated oxidative stress response markers (C) and mitochondrial unfolded protein response genes (D) in P*dat-1*::GFP neurons isolated from 1-day-old (young) and 5-day-old (aged) WT and *c30F12.2(ok3505)* transgenic animals. Data are mean±s.d. (*n*=5 biological replicates, each with *n*=4 technical replicates). (E) Movement of N2 and *c30F12.2(ok3505)* animals in liquid (thrashing) at day 1; *n*=3 with 25–30 animals per group. Data are mean±s.d. (F) Aldicarb-induced paralysis in age-matched N2 and *c30F12.2(ok3505)* worms at day 1. The animals were tested in three independent trials with 20 worms per group. Data are mean values±s.e.m. **P*<0.05, ***P*<0.01, ****P*<0.001 (*t*-test).

Oxidative damage has been previously shown to affect sensory neuronal function and has been implicated in age-dependent neurodegeneration (Minniti et al., 2009). However, *c30F12.2(ok3505)* mutants appeared normal in a number of sensory behavioral tests. They displayed normal positive (movement towards the attractive odorant diacetyl) and negative (movement away from the repulsive odorant ethanol) chemotaxis indexes (Fig. S7A), reflecting unaffected chemosensing. In addition, temperature-sensing appeared to be intact in *c30F12.2(ok3505)* animals, as did sensory release of serotonin. Increases in temperature-induced pharyngeal pumping rates, a function of temperature sensing by the AFD thermosensory neurons, and serotonin release by the serotonergic chemosensory ADF and neurosecretory NSM neurons remained unimpaired (Fig. S6D).

Journal of Cell Science (2018) 131, jcs219956. doi:10.1242/jcs.219956

c30F12.2(ok3505) mutants also did not undergo significant dopaminergic neuron degeneration with aging up to day 9 (Fig. S7B). This was surprising, as numerous studies have shown that dopaminergic neurons in *C. elegans* are particularly vulnerable to oxidative stress (Karbowski and Neutzner, 2012; Rugarli and Langer, 2012; Levytskyy et al., 2016). The GFP reporter used to assess the oxidative stress response of the organism is, for technical reasons, not active in *C. elegans* neurons. Therefore given these surprising results, we examined whether the neurons were indeed undergoing oxidative stress in the absence of LACE-1. To do this, we isolated specific groups of neurons from *C. elegans* strains, validated the enrichment of these cells by quantitative real-time PCR (qRT-PCR) analysis (Fig. S7C), and assessed gene expression changes in these neurons. *c30F12.2(ok3505)* animals were crossed with a series of established reporter strains allowing for specific expression of GFP reporter in dopaminergic neurons (^{P}*dat-1*::GFP), cholinergic neurons (^{P}*unc-17*::GFP), and muscle cells (^{P}*myo-3*::GFP); the animals were gently homogenized, and cells from control and *c30F12.2(ok3505)* reporter strains were separated by fluorescence-assisted cell sorting or via immunoisolation of GFP-expressing cells with anti-GFP magnetic beads (Fig. 8B; Fig. S7C). These isolated cell populations were used for RNA extractions and subsequent qRT-PCR analysis for evidence of oxidative stress. Consistent with a requirement for LACE-1 in the protection from oxidative stress, dopaminergic neurons from young adult and 5-day-old transgenic ^{P}*dat-1*::GFP control and *c30F12.2(ok3505)* worms indeed showed an increase in the expression of oxidative stress-responsive genes *sod-2*, *mtl-1*, and *hsp-16.2*, encoding mitochondrial superoxide dismutase, metallothionein and small heat shock protein, respectively (Fig. 8C). We next examined the transcript levels of canonical UPRmt genes by qRT-PCR. While no significant differences were seen in young animals, the neurons of older (day 5) *c30F12.2(ok3505)* animals displayed an ∼2-fold increase in the expression of *hsp-6*, *hsp-60* and *spg-7* UPRmt marker genes compared to the control strain (Fig. 8D). Interestingly, the expression of *lace-1* itself was increased ∼1.7-fold in ^{P}*dat-1*::GFP neurons and ∼1.3-fold in ^{P}*unc-17*::GFP neurons of 5-day-old WT worms when compared to young adult WT animals (Fig. S7D). In contrast, *lace-1* transcript levels were unchanged in ^{P}*myo-3*::GFP myocytes isolated from cells of the respective age-matched *C. elegans* strains (Fig. S7D) and in whole-worm extracts of young adult and 5-day-old animals. These data together indicate that, as with the whole animal, dopaminergic neurons were in fact undergoing enhanced oxidative stress with age, and this stress was exacerbated in the absence of LACE-1. However, notwithstanding the excess oxidative stress in dopaminergic neurons, our observation that ^{P}*dat-1*::GFP-labeled neurons in WT and *c30F12.2(ok3505)* animals did not degenerate even in animals as old as 9 days (Fig. S7B) suggests that the physiological effects of LACE-1 may be complex and specific to the cell type.

Although motility on solid substrates was normal (Fig. 8A), we did observe a slight, but significant impairment, in the 'thrashing' capacity of *c30F12.2(ok3505)* animals relative to control animals (Fig. 8E). This inability of animals to increase motility rates required to sustain movement in liquid media was coupled with deficits in acetylcholine neurotransmission in LACE-1-deficient animals, and *c30F12.2(ok3505)* animals showed an enhanced resistance to the acetylcholinesterase inhibitor aldicarb (Suo and Ishiura, 2013). While virtually all N2 worms were paralyzed after a 2-h treatment with 1 mM aldicarb, a large fraction of *c30F12.2(ok3505)* animals remained active, indicating an ∼1.7-fold increase in resistance to this neurotoxin (Fig. 8F). In sum, these studies taken together indicate that the function of the AAA ATPase LACE-1, while required to protect against oxidative stress and maintain mitochondrial protein homeostasis in multiple *C. elegans* tissues, is particularly important to maintain the functionality of specific *C. elegans* cells under conditions of high activity. Although it still remains to be determined, this inability of animals to adapt to environmental challenges and oxidative stress may result in the decrease in lifespan observed in the *c30F12.2(ok3505)* animals.

DISCUSSION

The present study reveals previously unrecognized roles for the conserved Afg1 AAA ATPase in establishing both matrix proteostasis and oxidative stress tolerance in yeast. We extend these findings to metazoans, demonstrating that the function of the enzyme is conserved in the roundworm genetic model. Furthermore, by focusing our analyses on physiological aspects of the *C. elegans* ortholog of Afg1, LACE-1, we show that its deficiency primarily manifests in neuromuscular phenotypes that appear to underlie reduced lifespan and enhanced sensitivity towards oxidative insults. These results establish a link between molecular aspects of Afg1/LACE-1 function and its physiological role in higher eukaryotes.

Our data are consistent with the previously proposed role for Afg1 in facilitating turnover of CcO subunits in yeast and mammalian cells (Khalimonchuk et al., 2007; Cesenkova et al., 2016a); however, several of the present results indicate that the function of Afg1 is more universal and not restricted to CcO maintenance. First, Afg1 overexpression rescues the profound high-temperature growth defect of a yeast strain lacking the key IMM proteases m-AAA and Oma1. The root cause of this impediment appears to be impaired IMM proteostasis and gross depolarization of *yta10Δ oma1Δ* mitochondria. Such defects are unlikely to be a mere consequence of impaired CcO function. This notion is further supported by the evolutionary conservation of Afg1 in organisms such as *Plasmodium*, which either completely lack CcO or are missing CcO subunits suspected to be Afg1 substrates. Second, the ability of high-copy Afg1 to compensate for the loss of mitochondrial Hsp70 chaperone or otherwise rescue its function strongly suggests that Afg1 can act more broadly and engage with different types of unfolded mitochondrial proteins. Of note, this result could potentially explain the observation by Cesnekova et al. suggesting a mammalian Afg1 ortholog has a role in mediating the mitochondrial import of p53 under stress (Cesenkova et al., 2016b). Finally, we show that Afg1 helps to alleviate deleterious effects caused by expression of the misfolding-prone mouse DHFR in the matrix. This result further indicates the broad selectivity of Afg1 towards misfolded proteins. In addition, and consistent with the previously reported association of Afg1 with the matrix side of the IMM (Khalimonchuk et al., 2007), these data reveal that the enzyme targets matrix-localized proteins and matrix-facing IMM proteins. This behavior is similar to that of the m-AAA and LON AAA proteases, which process both integral and peripheral IMM proteins (Korbel et al., 2004; Savel'ev et al., 1998; Major et al., 2006).

As a member of the classic AAA clade of AAA+ enzymes (Erzberger and Berger, 2006), Afg1 appears to share biochemical features typical for this family of protein-unfolding enzymes. The importance of the AAA structural features for Afg1 function is consistent with our observation that mutating key residues known to be critical for catalytic activity, substrate processing or enzymatic oligomerization yields Afg1 variants unable to reverse the phenotypes of the *afg1Δ* mutant or compensate for the loss of mitochondrial Hsp70. These results provide evidence that the

Journal of Cell Science (2018) 131, jcs219956. doi:10.1242/jcs.219956

ATPase function of Afg1 is critical for its role in mitochondrial homeostasis and support a model whereby this AAA enzyme uses ATP hydrolysis to fuel extraction and/or unfolding of proteins in the IMM or matrix.

Given the importance of Afg1 function, the modest mitochondrial dysfunction phenotype of the yeast *afg1*Δ mutant may seem counterintuitive; however, the lack of severity of this phenotype may instead imply the following. First, that Afg1 helps to clear basal, and presumably low, levels of misfolded proteins in the IMM or matrix sub-mitochondrial locale and only becomes limited when cells age or face severe homeostatic challenges. In line with this notion are the gradual nature of the acetate growth defect and the progressive oxidative inactivation of aconitase, both of which seem to arise from accumulating reactive oxygen species (ROS)-mediated damage. A recent study by Kardon et al. reported an unexpected role for the mitochondrial ClpX AAA ATPase as a chaperone for cofactor (pyridoxal phosphate) incorporation into 5-aminolevulinate synthase (Kardon et al., 2015), suggesting another possibility for the role of Afg1 might be to function in repair of oxidatively damaged 4Fe-4S cluster cofactors in aconitase. While, at present, we cannot completely rule out this possibility, our observation that the aconitase defect of *afg1*Δ cells cannot be corrected by exogenous iron supplementation (data not shown) argues against this scenario. Second, the function of Afg1 is likely overlapping with that of other MQC factors, which are known to exhibit a significant degree of functional redundancy. Consistent with this idea is the finding that there are additive genetic effects of *OMA1* and *PIM1* deletions in *afg1*Δ cells. Finally, yeast mitochondria appear to be tolerant towards a significant degree of mitochondrial depolarization and ROS, as reflected by the modest phenotypic manifestation in young *afg1*Δ mutant cells.

The ability of the previously uncharacterized *C. elegans* LACE-1 ortholog to efficiently replace yeast Afg1 is remarkable and, together with the high degree of similarity displayed by the enzyme in eukaryotes, suggests comparable activities and substrates for this enzyme in metazoans. Indeed, consistent with the role of Afg1 in mitochondrial proteostasis, we demonstrate that the depletion of LACE-1 impairs lifespan and oxidative stress tolerance and activates the mitochondrial unfolded protein response in *C. elegans*. Our study also reveals physiological penalties of LACE-1 deficiency in higher eukaryotes. In line with the observation that *lace-1* expression is elevated in worm neurons as these animals age, our data suggest that whole-animal *lace-1* deletion primarily affects neural circuitry-mediated responses. In this regard, LACE-1 may resemble another mitochondria-associated AAA ATPase, Msp1/ATAD, whose quality control activity was shown to be important for synaptic plasticity and behavior in rodents (Zhang et al., 2011). Based on our findings, we posit that *lace-1* activity is required for proper neurotransmitter transport/release or neuromuscular function. It is also possible that loss of *lace-1* expression may affect additional tissues via non-cell autonomous mechanisms, thereby affecting the health of the mutants. Further studies are warranted to clarify these issues. Interestingly, an earlier high-throughput study in *Drosophila melanogaster* identified the fly ortholog of Afg1/LACE-1, DmeI (CG8520), as being important for heat-induced pain perception (Neely et al., 2010). It is tempting to speculate that these traits may have common molecular underpinnings.

MATERIALS AND METHODS

Yeast strains and plasmids

Yeast strains used in this work are listed in Table S1. Strains that are unique to this study were generated by *in vivo* homologous recombination of relevant PCR-amplified gene-specific cassettes (Janke et al., 2004; Longtine et al., 1998). A plasmid harboring Afg1 with a C-terminal 6×His epitope tag was made by PCR amplification of the *AFG1* open-reading frame (ORF) from genomic DNA with flanking BamHI and PstI sites, followed by restriction enzyme cloning into pRS416 YCp and pRS426 YEp vectors under control of *MET25* promoter and *CYC1* terminator sequences. The E206Q, Y160A and L225D L226D mutations were made using the Q5 site-directed mutagenesis kit (New England Biolabs, Ipswich, MA). The LACE-1-6×His construct was PCR-amplified from *C. elegans* cDNA and cloned into pRS426 YEp vector under control of the *MET25* promoter and *CYC1* terminator. All constructs were validated by DNA sequencing. The vectors containing YTA10 E509Q (Arlt et al., 1996), YTA10 ΔTM (Korbel et al., 2004) and Cyb2-DHFR IMS- and matrix-targeted chimeric constructs, as well as their misfolding-prone variants (Vestweber and Schatz, 1988; Schreiner et al., 2012), have been described previously.

Yeast cell growth and assays

Cells were cultured at 28°C or 30°C in either yeast extract-peptone-dextrose (YPD, Amresco, Solon, OH) or Brent Supplement Mixture synthetic selective medium (SC, Sunrise Science Products, San Diego, CA) when necessary to maintain plasmid selection in transformed cells. For growth assays, cultures were grown for the indicated periods of time, adjusted to an absorbance at 600 nm (A_{600}) of 0.5, serially diluted (10-fold dilutions), and spotted onto media plates. For the colony-forming unit assessment, cells were handled and analyzed as previously reported (Bohovych et al., 2014, 2015b).

Oxygen consumption was measured in whole cells in the presence of galactose with an Oxygraph instrument (Hansatech Instruments, Pentney, UK), and the rates were calculated as per the manufacturer's instructions from the linear response. Mitochondrial membrane potential and ROS level measurements were performed via fluorescence-activated cell sorting (FACS) analysis of stained samples essentially as previously described (Khalimonchuk et al., 2012). Briefly, synchronized cells were grown until mid-logarithmic phase (A_{600} of 0.5) or aged for 24 h after synchronization for stationary phase cells. Washed cells were treated with the mitochondrial membrane potential probe JC-1 (5 µM) for 10 min at 30°C then measured via FACS as described by the manufacturer (Thermo Fisher Scientific, Waltham, MA). ROS, specifically superoxide levels, were measured using dihydroethidium (DHE), a superoxide-specific indicator (Thermo Fisher Scientific). Similar to above, cells were grown until mid-logarithmic phase, treated with 10 µM DHE for 20 min at 30°C, and measured according to the manufacturer's protocol (Thermo Fisher Scientific).

Yeast mitochondrial isolation and analysis

Yeast mitochondria were isolated according to published procedures (Diekert et al., 2001). Total mitochondrial protein concentration was determined by the Bradford method by using the Coomassie Plus assay kit (Thermo Fisher Scientific). Specific enzymatic activities of aconitase, succinate dehydrogenase, cytochrome *c* oxidase, cytochrome bc_1 complex and superoxide dismutase were determined from mitochondrial lysates as previously described (Barrientos, 2002; Salomé et al., 2013). The oligomeric states of Afg1 variants were assessed by high-velocity fractionation of mitochondrial lysates using a 12–50% continuous sucrose gradient as described previously (Swenson et al., 2016; Khalimonchuk et al., 2010).

Immunoblotting

Blue native (BN)-PAGE separation of mitochondrial protein complexes solubilized with 1% digitonin was performed as described previously (Swenson et al., 2016; Khalimonchuk et al., 2010) using 3–12% gradient polyacrylamide gels (Life Technologies, Inc., Carlsbad, CA). SDS-PAGE- or BN-PAGE-separated proteins from mitochondrial lysates were transferred onto nitrocellulose or PVDF membranes and blocked with 5% nonfat milk-PBS (with or without 0.1% Tween 20). Protein bands of interest were detected by probing membranes with the following primary antibodies: rabbit anti-Aco1 (1:5000, a kind gift from Roland Lill, Institute for Cell Biology and Cytopathology, University of Marburg, Germany); mouse anti-porin (1:7500, 459500, Invitrogen, Carlsbad, CA); rabbit anti-Sod1 and anti-Sod2 (both at 1:5000; kind gifts from Valeria Culotta, Department of Biochemistry and Molecular Biology, Johns Hopkins University, USA);

mouse anti-6×His epitope (1:2000, MA1-21315, Thermo Fisher Scientific); mouse anti-DHFR (1:5000, MAB7934, R&D Systems, Minneapolis, MN); mouse anti-Cox1 (1:2000, ab110270, Abcam, Cambridge, UK); mouse anti-Cox2 (1:2000, ab110271, Abcam); mouse anti-Cox3 (1:2000, ab110259, Abcam); mouse anti-Rip1, rabbit anti-Sdh2, and rabbit anti-Cyt1 (1:2000, 1:5000 and 1:3000, respectively; kind gifts from Dennis Winge, Department of Internal Medicine, University of Utah Health Science Center, USA); and rabbit anti-Atp2 β subunit of F_1 (1:5000, a kind gift from Alexander Tzagoloff, Columbia University, USA) antibodies. The secondary horseradish peroxidase (HRP)-coupled goat anti-mouse IgG antibodies were from Jackson ImmunoResearch Laboratories (West Grove, PA, 115-035-068) or Santa Cruz Biotechnology (Dallas, TX, sc-2005), and the similarly coupled goat anti-rabbit IgG antibodies were from Cell Signaling Technology (Danvers, MA, 7074S) or Santa Cruz Biotechnology (sc-2030). The protein–antibody conjugates were visualized using chemiluminescence reagents (Thermo Fisher Scientific, Millipore, or Bio-Rad) and either X-ray film (Phenix Research Products, Candler, NC) or an Amersham Imager 600 (GE Healthcare, Little Chalfont, UK). Note that the Amersham camera imager, unlike film, does not produce noticeable background darkening unless a very long exposure is used; short exposures capture bands from the presence of HRP-coupled secondary antibody against a white background.

C. elegans strains

The *C. elegans* strains used in this study were Bristol N2 and *c30F12.2(ok3505)*. These strains and the ^{P}*dat-1::*GFP and ^{P}*unc-17::*GFP reporter strains were kindly provided by the *Caenorhabditis* Genetics Center (CGC) at the University of Minnesota. The ^{P}*hsp-60::*GFP, ^{P}*hsp-6::*GFP, ^{P}*spg-7::*GFP, ^{P}*myo-3::*GFP, and ^{P}*myo-3::*mitoGFP reporter strains were kindly provided by Cole Haynes (University of Massachusetts Medical Center, USA). The LACE-1-deficient reporter lines were generated by genetic crosses with the *c30F12.2(ok3505)* strain and confirmed by back-cross and PCR analysis. For the comparison of WT and mutant worm strains, the animals were analyzed in young adult and 5-day-old growth stages, unless stated otherwise.

Worm growth and physiological assays

All worm strains were cultured at 20°C and maintained at low densities under standard conditions (Stiernagle, 2006). Worms were fed with *E. coli* OP50 cells (obtained from the CGC) that were seeded onto nematode growth medium (NGM) plates 2 days prior to use. Unless indicated otherwise, all animals tested in our assays were 1-day- or 5-day-old adult hermaphrodites.

Egg laying was assessed by moving individual animals onto fresh plates every day starting from L4 stage animals until day 5 of adulthood. The plates were examined for dead eggs, and progeny that hatched were scored when they developed into L4 stage larvae.

RNA interference experiments were carried out using the standard RNAi feeding protocol (Hart, 2006). The bacterial clone expressing pL4440 control RNAi vector was obtained from the CGC; the *lace-1* (*c30F12.2*) dsRNA-expressing construct was generated by cloning the respective sequence into pL4440 RNAi vector via PCR of *C. elegans* cDNA with flanking regions containing NotI and XbaI restriction sites. All RNAi clones used in this study were verified by sequencing. RNAi genetic knockdown was achieved by feeding worms for 3 days.

Lifespan was determined on OP50-seeded NGM plates supplemented with 25 µM 5-fluoro-2′-deoxyuridine (FUdR) to limit the growth of progeny in the first generation. Synchronized worms were transferred onto fresh plates after 2 days of culturing to avoid starvation and prevent progeny formation; the transfers were performed until the animals were no longer able to reproduce. Viability of the animals was monitored every 2 days by gentle tapping of the plate or by touching the medium near the worm. Animals that died through internal hatching of progeny were not considered.

Worm oxidative stress resistance

Standard NGM plates with 5 µM rotenone were used for the worm oxidative stress resistance assay. Rotenone was dissolved in DMSO, and control plates poured at the same time had vehicle only. Adult N2 and *c30F12.2(ok3505)* animals were bleached, and eggs were spread on an empty NGM plate for ∼18 h. Approximately 100–150 hatched L1 stage animals were placed on rotenone plates and scored every subsequent day for their developmental stage. Since assessing the stages earlier than L4 was inefficient under the dissecting microscope, animals were classified as being below, at or above L4 stage. The percentage of animals in each growth category was calculated across three biological replicates.

Worm behavioral assays

Motility assays on NGM plates were performed as follows. Ten L4-stage animals of each strain were picked 24–26 h prior to the assay and allowed to mature into adults. Plates with 1-day-old animals were allowed 1 h to acclimatize to room temperature prior to the experiment and then worms were transferred, by picking, to the center of a fresh plate and their motility recorded for a duration of 1 min. The distance moved by each animal was then measured manually using ImageJ (National Institutes of Health).

To measure pumping rates, 10 L4-stage worms of each strain were picked and transferred to new NGM plates. After 24–28 h, the resulting 1-day-old adults were transferred singly onto fresh plates and allowed to acclimatize for 30–90 min. Pharyngeal movements were recorded while viewing animals under a MZ10F stereomicroscope (Leica Camera AG, Wetzlar, Germany) at 8× magnification. Pumping rates were recorded as the number of pharyngeal pumps each worm performed in a 10-s time period. Three simultaneous recordings were taken, averaged, and multiplied by six to get the average number of pumps per minute. For basal pumping rates, the room temperature was maintained at 20–22°C and continuously monitored. Pumping rates under increased temperatures were measured by placing the plates on a Peltier-heated stage (PeCon GmbH Temp Controller, model no. 2000-2, Erbach, Germany) that was equilibrated to 34°C prior to the experiment as previously described (Tatum et al., 2015).

For thrashing assays, 25–30 age-matched animals were placed into a 50-µl drop of M9 buffer and allowed to acclimatize for 2 min. Mid-body movement rates (thrashing) were recorded while viewing animals under a SMT1-FLQC fluorescence stereomicroscope (Tritech Research, Los Angeles, CA). Three simultaneous recordings were made per each biological replicate.

Chemotaxis assays were performed according to modified versions of previously published protocols (Hart, 2006; Cooper et al., 2015) at room temperature. For each of the chemotaxis assays, three sets of 20 animals of each strain were picked as L4 stage animals at 24–26 h prior to the assay, allowed 1 h to acclimatize to room temperature prior to the experiment, and then transferred, by picking, to the appropriate chemotaxis plate. For chemoattraction towards diacetyl (Alfa Aesar, Haverhill, MA), a 0.01% solution of diacetyl diluted in water mixed with 0.5 M sodium azide was spotted on two of four quadrants of the plate. For the ethanol chemoaversion assays, 50 µl ethanol mixed with sodium azide was applied to two quadrants of a plate. Water mixed with sodium azide was used as the control odorant. Worms were placed in the center of the assay plate and allowed to move for 30 min, at which point the entire plate was imaged and the worms were scored for their quadrant of preference. A chemotaxis index was calculated using the following equation:

$$\frac{(\#\text{ of animals on experimental odor}) - (\#\text{ of animals on control odor})}{(\#\text{ of animals on experimental odor}) + (\#\text{ of animals on control odor})}.$$

The resistance to aldicarb was assessed according to previously published protocols (Mahoney et al., 2006). In brief, 0.5 mM aldicarb [2-methyl-2-(methylthio)propionaldehyde O-(methylcarbamoyl)-oxime, Sigma-Aldrich, St. Louis, MO] was dissolved in 70% ethanol, and added to the NGM plates and allowed to dry overnight. Similar volumes of ethanol alone were used as a control. The plates were then seeded with 50 µl OP50 and allowed to dry for 4–6 h. Three sets of 20 L4 animals of each strain were picked onto plates 24–26 h prior to the experiment and allowed to mature into day 1 adults. Animals were then placed on the OP50 lawn and scored by a researcher that was blind to the experimental condition for paralysis every 30 min for a 2-h period. Animals were considered paralyzed when they failed to move despite being prodded three times with a platinum wire.

Isolation of GFP-tagged cell populations from worms

Worms were grown until L4 stage or aged on NGM containing 25 µM FUdR for 5 days, and populations of GFP-expressing cells were isolated as previously described (Zhang et al., 2011) with minor modifications. The animals were washed with M9 buffer, resuspended in SDS-DTT buffer (200 mM DTT, 0.25% SDS, 3% sucrose, 20 mM HEPES, pH 8.0), and incubated for 5 min at room temperature. Egg buffer (800 µl; 118 mM NaCl, 48 mM KCl, 2 mM CaCl, 2 mM $MgCl_2$, 25 mM HEPES, pH 7.3) was added and the samples mixed gently. Worms were pelleted for 1 min at 15,000 ***g*** and washed with egg buffer; this was repeated five times. Pronase (10 µl) was added to pellets followed by incubation for 10 min, during which worms were ground up using a pipette tip. After 10 min, 900 µl of M9 buffer was added to stop the reaction. Cells were pelleted via centrifugation for 5 min at 9500 ***g*** at 4°C. The supernatant was removed, and pellets were resuspended in M9 buffer and used in FACS-based cell sorting as described (Zhang et al., 2011). Alternatively, anti-GFP-conjugated magnetic beads were used to isolate the cells (pellets were resuspended in 35 µl of M9 buffer, and 15 µl of magnetic anti-GFP beads were added and incubated at 4°C for 1 h then washed with 100 µl M9 buffer three times). RNA isolation then followed.

Worm mitochondrial isolation

Mitochondria isolation from worms was performed essentially as described previously (Rao et al., 2005). Worms were collected and resuspended in breaking buffer (50 mM Tris-HCl, 150 mM NaCl, 1 mM EDTA, 5 mM DTT and 1 mM PMSF) and a French press was used to lyse the worms via three passes at 10,000 psi with 15 s sonication after each pass. The lysate was then centrifuged at 10,000 ***g*** for 10 min at 4°C. The pellet was resuspended in mito buffer (0.65 M sorbitol, 1 mM PMSF, 10 mM Tris-HCl, pH 7.4) and centrifuged at 4500 ***g*** for 5 min at 4°C. The supernatant was collected, centrifuged at 10,000 ***g*** for 10 min at 4°C, and the pellet containing isolated mitochondria was resuspended in mito buffer.

Gene expression analysis

C. elegans total RNA was isolated by the TRIzol method as previously described (Morley and Morimoto, 2004). Yeast total RNA was isolated with a RNA purification kit (Epicentre, Madison, WI) following the manufacturer's protocol. cDNAs were produced using the iScript cDNA synthesis kit (Bio-Rad, Hercules, CA). qRT-PCR was performed per manufacturer's instructions in an iCycler Real-Time PCR detection system with SYBR green master mix (Bio-Rad). The relative amounts of relevant transcripts were determined using the $\Delta\Delta C_t$ method and normalized to the expression levels of the *act-3* gene. The sequences of primers used in these analyses are available upon request.

Microscopy analysis

Yeast cells expressing Su9–RFP mitochondrial marker were grown at 28°C to mid-log phase in YPD or SC medium and then split into two cultures; one was further cultured at 28°C and the other was shifted to 37°C for 6 h. Following the incubation, the cells were imaged using an Olympus IX81-FV5000 confocal laser-scanning microscope (Olympus America, Center Valley, PA) with a 100× oil objective. Images were acquired and processed with the FluoView 500 software package (Olympus America).

For high-resolution worm imaging, synchronized animals were anesthetized with 2 mM levamisole and placed on 5% agarose on glass slides. The images were acquired using an Olympus IX81-FV5000 microscope with a 100× objective. Several z-stack images were collected and processed using the FluoView 500 software. For low-resolution fluorescent imaging, we used an upright SMT1-FLQC fluorescence stereomicroscope system (Tritech Research) and 5.0 MP 1/3″ CCD color digital video camera (Sony Corp., Tokyo, Japan).

Statistical analysis

All statistical analyses and graphing were performed using Microsoft Excel or KaleidaGraph software. The parametric Student's *t*-test or one-way ANOVA analysis with post-hoc Tukey's range test were used to determine significance. Overall, $P<0.05$ was considered statistically significant. At least three independent replicates were obtained for each represented experiment or dataset.

Acknowledgements

We thank I. Bohovych and S. Swenson for their help with yeast stress assays; N. Harris and H. Ferro for previous work on this project; and D. Mokranjac (Ludwig-Maximilians University), A. Barrientos (University of Miami), T. Langer (University of Cologne), J. Shaw (University of Utah), T. Fox (Cornell University), R. Lill (Marburg University), V. Culotta (Johns Hopkins University), A. Tzagoloff (Columbia University), D. Winge (University of Utah) and C. Haynes (University of Massachusetts Medical School) for strains and reagents. We thank the *Caenorhabditis* Genetics Center at the University of Minnesota for the c30F12.2(ok3505) strain and other reagents.

Competing interests

The authors declare no competing or financial interests.

Author contributions

Conceptualization: E.M.G., J.L.F., V.P., O.K.; Methodology: E.M.G., J.L.F., V.P., O.K.; Validation: J.L.F., O.K.; Formal analysis: J.L.F., O.K.; Investigation: E.M.G., N.Z., M.L.H., J.L.F., V.P., O.K.; Resources: J.L.F., V.P., O.K.; Writing - original draft: J.L.F., O.K.; Writing - review & editing: J.L.F., V.P., O.K.; Visualization: N.Z., M.L.H., J.L.F., V.P., O.K.; Supervision: J.L.F., O.K.; Project administration: J.L.F., O.K.; Funding acquisition: J.L.F., O.K.

Funding

This work was supported by the National Institutes of Health (R01GM108975 to O.K., P30GM103335 to O.K. via Nebraska Redox Biology Center, R01AG050653 to V.P., T32 GM107001-01A1 to E.M.G., 5 P20 RR016461, and 8 P20 GM103499), Research Corporation for Science Advancement (Cottrell College Science Award 22643 to J.L.F.), the Howard Hughes Medical Institute (52007537 through the Pre-college & Undergraduate Science Education Program), and the College of Charleston (Summer Undergraduate Research with Faculty grant SU2017-007 to M.L.H. and J.L.F.). The content is solely the responsibility of the authors and does not necessarily represent the official views of the National Institutes of Health. Deposited in PMC for release after 12 months.

Supplementary information

Supplementary information available online at http://jcs.biologists.org/lookup/doi/10.1242/jcs.219956.supplemental

References

Abrahams, B. S., Mak, G. M., Berry, M. L., Palmquist, D. L., Saionz, J. R., Tay, A., Tan, Y. H., Brenner, S., Simpson, E. M. and Venkatesh, B. (2002). Novel vertebrate genes and putative regulatory elements identified at kidney disease and NR2E1/fierce loci. *Genomics* **80**, 45-53.

Al-Furoukh, N., Kardon, J. R., Krüger, M., Szibor, M., Baker, T. A. and Braun, T. (2014). NOA1, a novel ClpXP substrate, takes an unexpected nuclear detour prior to mitochondrial import. *PLoS ONE* **9**, e103141.

Arlt, H., Tauer, R., Feldmann, H., Neupert, W. and Langer, T. (1996). The YTA10-12 complex, an AAA protease with chaperone-like activity in the inner membrane of mitochondria. *Cell* **85**, 875-885.

Babu, M., Vlasblom, J., Pu, S., Guo, X., Graham, C., Bean, B. D. M., Burston, H. E., Vizeacoumar, F. J., Snider, J., Phanse, S. et al. (2012). Interaction landscape of membrane-protein complexes in Saccharomyces cerevisiae. *Nature* **489**, 585-589.

Bárcena, C., Mayoral, P. and Quirós, P. M. (2018). Mitohormesis, an antiaging paradigm. *Int. Rev. Cell Mol. Biol.* **340**, 35-77.

Barrientos, A. (2002). *In vivo* and *in organello* assessment of OXPHOS activities. *Methods* **26**, 307-316.

Barthelme, D. and Sauer, R. T. (2012). Identification of the Cdc48-20S Proteasome as an ancient AAA+ proteolytic machine. *Science* **337**, 843-846.

Bender, T., Leidhold, C., Ruppert, T., Franken, S. and Voos, W. (2010). The role of protein quality control in mitochondrial protein homeostasis under oxidative stress. *Proteomics* **10**, 1426-1443.

Bennett, C. F., Vander Wende, H., Simko, M., Klum, S., Barfield, S., Choi, H., Pineda, V. V. and Kaeberlein, M. (2014). Activation of the mitochondrial unfolded protein response does not predict longevity in *Caenorhabditis elegans*. *Nat. Commun.* **5**, 3483.

Bohovych, I., Donaldson, G., Christianson, S., Zahayko, N. and Khalimonchuk, O. (2014). Stress-triggered activation of the metalloprotease Oma1 involves its C-terminal region and is important for mitochondrial stress protection in yeast. *J. Biol. Chem.* **289**, 13259-13272.

Bohovych, I., Chan, S. S. L. and Khalimonchuk, O. (2015a). Mitochondrial protein quality control: the mechanisms guarding mitochondrial health. *Antioxid. Redox Signal.* **22**, 977-994.

Bohovych, I., Fernandez, M. R., Rahn, J. J., Stakley, K. D., Bestman, J. E., Anandhan, A., Franco, R., Claypool, S. M., Lewis, R. E., Chan, S. S. L. et al. (2015b). Metalloprotease OMA1 fine-tunes mitochondrial bioenergetic function and respiratory supercomplex stability. *Sci. Rep.* **5**, 13989.

Bota, D. A., Van Remmen, H. and Davies, K. J. A. (2002). Modulation of Lon protease activity and aconitase turnover during aging and oxidative stress. *FEBS Lett.* **532**, 103-106.

Burté, F., Carelli, V., Chinnery, P. F. and Yu-Wai-Man, P. (2015). Disturbed mitochondrial dynamics and neurodegenerative disorders. *Nat. Rev. Neurol.* **11**, 11-24.

Cesenkova, J., Rodinova, M., Hansikova, H., Houstek, J., Zeman, J. and Stiburek, L. (2016a). The mammalian homologue of yeast Afg1 ATPase (lactation elevated 1) mediates degradation of nuclear-encoded complex IV subunits. *Biochem. J.* **473**, 797-804.

Cesenkova, J., Spacilova, J., Hansikova, H., Houstek, J., Zeman, J. and Stiburek, L. (2016b). LACE1 interacts with p53 and mediates its mitochondrial translocation and apoptosis. *Oncotarget* **7**, 47687-47698.

Chen, Y.-C., Umanah, G. K. E., Dephoure, N., Andrabi, S. A., Gygi, S. P., Dawson, T. M., Dawson, V. L. and Rutter, J. (2014). Msp1/ATAD1 maintains mitochondrial function by facilitating the degradation of mislocalized tail-anchored proteins. *EMBO J.* **33**, 1548-1564.

Cooper, J. F., Dues, D. J., Spielbauer, K. K., Machiela, E., Senchuk, M. M. and Van Raamsdonk, J. M. (2015). Delaying aging is neuroprotective in Parkinson's disease: a genetic analysis in *C. elegans* models. *NPJ Parkinsons Dis.* **1**, 15022.

Dekker, P. J. T., Martin, F., Maarse, A. C., Bomer, U., Muller, H., Guiard, B., Rassow, J. and Pfanner, N. (1997). The Tim core complex defines the number of mitochondrial translocation contact sites and can hold arrested preproteins in the absence of matrix Hsp70-Tim44. *EMBO J.* **16**, 5408-5419.

Diekert, K., de Kroon, A. I., Kispal, G. and Lill, R. (2001). Isolation and subfractionation of mitochondria from the yeast *Saccharomyces cerevisiae*. *Methods Cell Biol.* **65**, 37-51.

Erzberger, J. P. and Berger, J. M. (2006). Evolutionary relationships and structural mechanisms of AAA+ proteins. *Annu. Rev. Biophys. Biomol. Struct.* **35**, 93-114.

Gardner, P. R., Nguyen, D. D. and White, C. W. (1994). Aconitase is a sensitive and critical target of oxygen poisoning in cultured mammalian cells and in rat lungs. *Proc. Natl. Acad. Sci. USA* **91**, 12248-12252.

Glynn, S. E. (2017). Multifunctional mitochondrial AAA proteases. *Font. Mol. Biosci.* **4**, 34.

Hart, A. C. (ed.) (2006). Behavior. In *WormBook: The Online Review of C. elegans Biology* (ed. **The C. elegans Research Community**). http://www.wormbook.org.

Janke, C., Magiera, M. M., Rathfelder, N., Taxis, C., Reber, S., Maekawa, H., Moreno-Borchart, A., Doenges, G., Schwob, E., Schiebel, E. et al. (2004). A versatile toolbox for PCR-based tagging of yeast genes: new fluorescent proteins, more markers and promoter substitution cassettes. *Yeast* **21**, 947-962.

Kang, P.-J., Ostermann, J., Shilling, J., Neupert, W., Craig, E. A. and Pfanner, N. (1990). Requirement for hsp70 in the mitochondrial matrix for translocation and folding of precursor proteins. *Nature* **348**, 137-143.

Kang, S. G., Ortega, J., Singh, S. K., Wang, N., Huang, N.-N., Steven, A. C. and Maurizi, M. R. (2002). Functional proteolytic complexes of the human mitochondrial ATP-dependent protease, hClpXP. *J. Biol. Chem.* **277**, 21095-21102.

Karbowski, M. and Neutzner, A. (2012). Neurodegeneration as a consequence of failed mitochondrial maintenance. *Acta Neuropathol.* **123**, 157-171.

Kardon, J. R., Yien, Y. Y., Huston, N. C., Branco, D. S., Hildick-Smith, G. J., Rhee, K. Y., Paw, B. H. and Baker, T. A. (2015). Mitochondrial ClpX activates a key enzyme for heme biosynthesis and erythropoiesis. *Cell* **161**, 858-867.

Khalimonchuk, O., Bird, A. and Winge, D. R. (2007). Evidence for a pro-oxidant intermediate in the assembly of cytochrome oxidase. *J. Biol. Chem.* **282**, 17442-17449.

Khalimonchuk, O., Bestwick, M., Meunier, B., Watts, T. C. and Winge, D. R. (2010). Formation of the redox cofactor centers during Cox1 maturation in yeast cytochrome oxidase. *Mol. Cell. Biol.* **30**, 1004-1017.

Khalimonchuk, O., Jeong, M.-Y., Watts, T., Ferris, E. and Winge, D. R. (2012). Selective Oma1 protease-mediated proteolysis of Cox1 subunit of cytochrome oxidase in assembly mutants. *J. Biol. Chem.* **287**, 7289-7300.

Korbel, D., Wurth, S., Käser, M. and Langer, T. (2004). Membrane protein turnover by the m-AAA protease in mitochondria depends on the transmembrane domains of its subunits. *EMBO Rep.* **5**, 698-703.

Lee, Y.-J. and Wickner, R. B. (1992). AFG1, a new member of the SEC18-NSF, PAS1, CDC48-VCP, TBP family of ATPases. *Yeast* **8**, 787-790.

Levytskyy, R. M., Germany, E. M. and Khalimonchuk, O. (2016). Mitochondrial quality control proteases in neuronal welfare. *J. Neuroimmune Pharmacol.* **11**, 629-644.

Lin, M. T. and Beal, M. F. (2006). Mitochondrial dysfunction and oxidative stress in neurodegenerative diseases. *Nature* **443**, 787-795.

Longtine, M. S., McKenzie, A., III, Demarini, D. J., Shah, N. G., Wach, A., Brachat, A., Philippsen, P. and Pringle, J. R. (1998). Additional modules for versatile and economical PCR-based gene deletion and modification in Saccharomyces cerevisiae. *Yeast* **14**, 953-961.

Mahoney, T. R., Luo, S. and Nonet, M. L. (2006). Analysis of synaptic transmission in *Caenorhabditis elegans* using an aldicarb-sensitivity assay. *Nat. Protoc.* **1**, 1772-1777.

Major, T., von Janowsky, B., Ruppert, T., Mogk, A. and Voos, W. (2006). Proteomic analysis of mitochondrial protein turnover: identification of novel substrate proteins of the matrix protease pim1. *Mol. Cell. Biol.* **26**, 762-776.

Minniti, A. N., Cataldo, R., Trigo, C., Vasquez, L., Mujica, P., Leighton, F., Inestrosa, N. C. and Aldunate, R. (2009). Methionine sulfoxide reductase A expression is regulated by the DAF-16/FOXO pathway in *Caenorhabditis elegans*. *Aging Cell* **8**, 690-705.

Morley, J. F. and Morimoto, R. I. (2004). Regulation of longevity in *Caenorhabditis elegans* by heat shock factor and molecular chaperones. *Mol. Biol. Cell* **15**, 657-664.

Neely, G. G., Hess, A., Costigan, M., Keene, A. C., Goulas, S., Langeslag, M., Griffin, R. S., Belfer, I., Dai, F., Smith, S. B. et al. (2010). A genome-wide Drosophila screen for heat nociception identifies $\alpha2\delta3$ as an evolutionarily conserved pain gene. *Cell* **143**, 628-638.

Neupert, W. and Herrmann, J. M. (2007). Translocation of proteins into mitochondria. *Annu. Rev. Biochem.* **76**, 723-749.

Okreglak, V. and Walter, P. (2014). The conserved AAA-ATPase Msp1 confers organelle specificity to tail-anchored proteins. *Proc. Natl. Acad. Sci. USA* **111**, 8019-8024.

Perez-Martinez, X., Broadley, S. A. and Fox, T. D. (2003). Mss51p promotes mitochondrial Cox1p synthesis and interacts with newly synthesized Cox1p. *EMBO J.* **22**, 5951-5961.

Rao, A. U., Carta, L. K., Lesuisse, E. and Hamza, I. (2005). Lack of heme synthesis in a free-living eukaryote. *Proc. Natl. Acad. Sci. USA* **102**, 4270-4275.

Rugarli, E. I. and Langer, T. (2012). Mitochondrial quality control: a matter of life and death for neurons. *EMBO J.* **31**, 1336-1349.

Salomé, P. A., Oliva, M., Weigal, D. and Krämer, U. (2013). Circadian clock adjustment to plant iron status depends on chloroplast and phytochrome functions. *EMBO J.* **20**, 511-523.

Sauer, R. T. and Baker, T. A. (2011). AAA+ proteases: ATP-fueled machines of protein destruction. *Annu. Rev. Biochem.* **80**, 587-612.

Savel'ev, A. S., Novikova, L. A., Kovaleva, I. E., Luzikov, V. N., Neupert, W. and Langer, T. (1998). ATP-dependent proteolysis in mitochondria. m-AAA protease and PIM1 protease exert overlapping substrate specificities and cooperate with the mtHsp70 system. *J. Biol Chem.* **273**, 20596-20602.

Schreiner, B., Westerburg, H., Forné, I., Imhof, A., Neupert, W. and Mokranjac, D. (2012). Role of the AAA protease Yme1 in folding of proteins in the intermembrane space of mitochondria. *Mol. Biol. Cell* **23**, 4335-4346.

Stefely, J. A., Kwiecien, N. W., Freiberger, E. C., Richards, A. L., Jochem, A., Rush, M. J. P., Ulbrich, A., Robinson, K. P., Hutchins, P. D., Veling, M. T. et al. (2016). Mitochondrial protein functions elucidated by multi-omic mass spectrometry profiling. *Nat. Biotechnol.* **34**, 1191-1197.

Stiernagle, T. (2006). Maintenance of *C. elegans*. In *WormBook: The Online Review of C. elegans Biology* (ed. **The C. elegans Research Community**). http://www.wormbook.org.

Suo, S. and Ishiura, S. (2013). Dopamine modulates acetylcholine release via octopamine and CREB signaling in *Caenorhabditis elegans*. *PLoS ONE* **8**, e72578.

Swenson, S., Cannon, A., Harris, N. J., Taylor, N. G., Fox, J. L. and Khalimonchuk, O. (2016). Analysis of oligomerization properties of heme *a* synthase provides insights into its function in eukaryotes. *J. Biol. Chem.* **291**, 10411-10425.

Tatum, M. C., Ooi, F. K., Chikka, M. R., Chauve, L., Martinez-Velazquez, L. A., Steinbusch, H. W. M., Morimoto, R. I. and Prahlad, V. (2015). Neuronal serotonin release triggers the heat shock response in C. elegans in the absence of temperature increase. *Curr. Biol.* **25**, 163-174.

Taylor, N. G., Swenson, S., Harris, N. J., Germany, E. M., Fox, J. L. and Khalimonchuk, O. (2017). The assembly factor Pet117 couples heme *a* synthase activity to cytochrome oxidase assembly. *J. Biol. Chem.* **292**, 1815-1825.

Vestweber, D. and Schatz, G. (1988). Point mutations destabilizing a precursor protein enhance its post-translational import into mitochondria. *EMBO J.* **7**, 1147-1151.

Wagener, N., Ackermann, M., Funes, S. and Neupert, W. (2011). A pathway for translocation in mitochondria by the AAA-ATPase Bcs1. *Mol. Cell* **44**, 191-202.

Wallace, D. C. (2013). A mitochondrial bioenergetics etiology of disease. *J. Clin. Invest.* **123**, 1405-1412.

Weir, N. R., Kamber, R. A., Martenson, J. S. and Denic, V. (2017). The AAA protein Msp1 mediates clearance of excess tail-anchored proteins from the peroxisomal membrane. *elife* **6**, e28507.

Wohlever, M. L., Mateja, A., McGilvray, P. T., Day, K. J. and Keenan, R. J. (2017). Msp1 is a membrane protein dislocase for tail-anchored proteins. *Mol. Cell* **67**, 194-202.e6.

Zhang, J., Wang, Y., Chi, Z., Keuss, M. J., Pai, Y.-M. E., Kang, H. C., Shin, J.-H., Bugayenko, A., Wang, H., Xiong, Y. et al. (2011). The AAA+ ATPase Thorase regulates AMPA receptor-dependent synaptic plasticity and behavior. *Cell* **145**, 284-299.

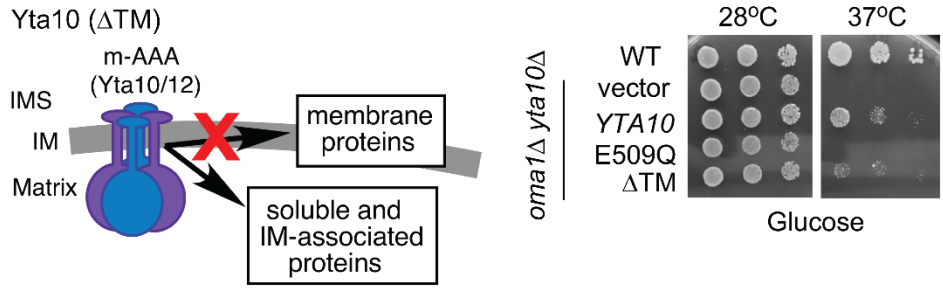

Figure S1. Simultaneous loss of Oma1 and Yta10 impairs proteolysis of intrinsic IM proteins. Left, schematic depiction of functional impairment in the m-AAA protease harboring the Yta10(ΔTM) subunit lacking transmembrane segments. Right, fermentative growth of WT or *oma1*Δ *yta10*Δ cells expressing the indicated Yta10 variants, handled and analyzed as in Figure 1A.

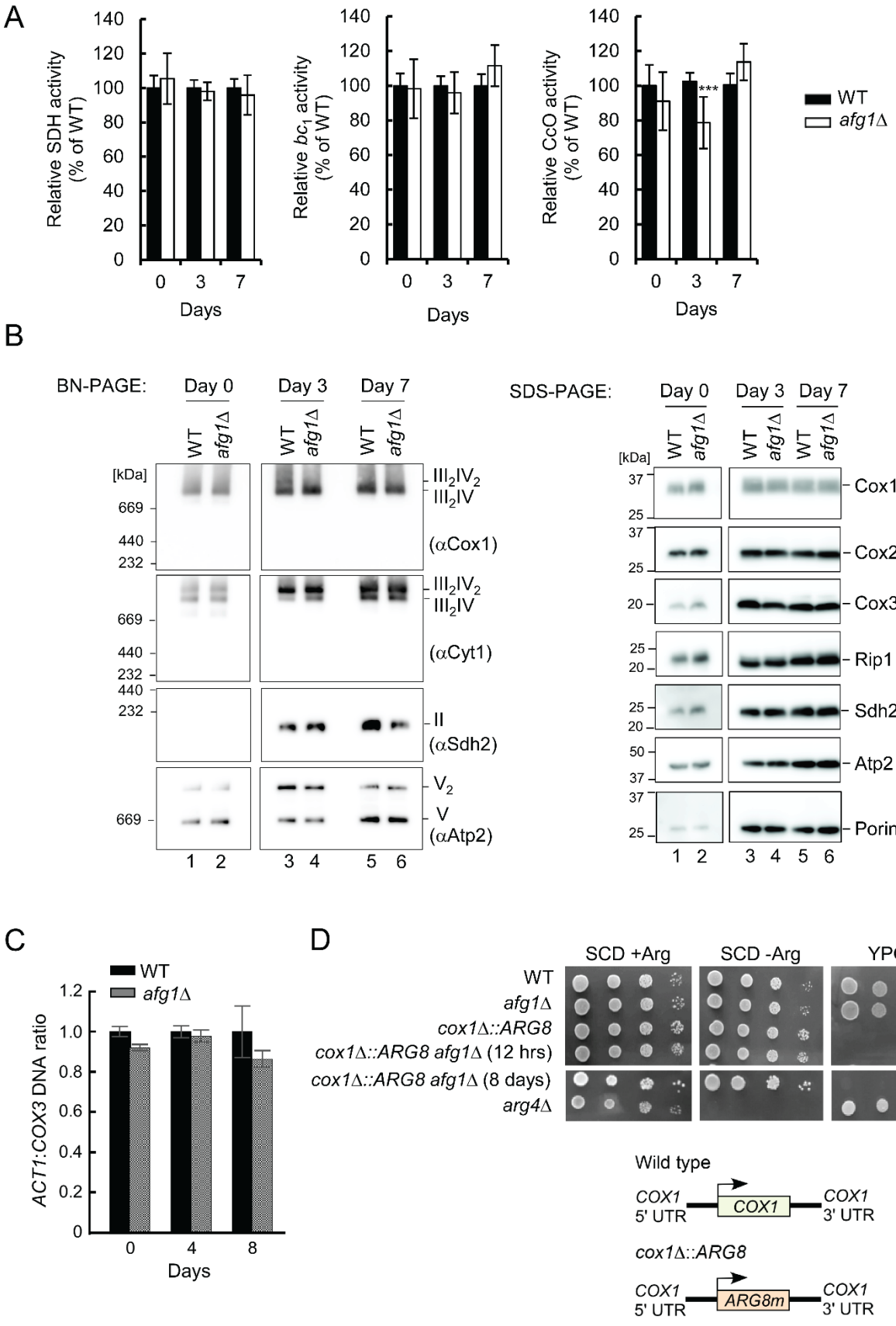

Figure S2. ETC enzymatic activities, complexes, and subunits in the absence of Afg1 are similar to WT, and cells lacking Afg1 retain mitochondrial genome with aging, similarly to WT. (A) Succinate dehydrogenase (SDH), cytochrome bc_1 complex (bc_1), and cytochrome *c* oxidase (CcO) specific enzymatic activities in mitochondria from WT and *afg1*Δ cells isolated at indicated growth times, shown as a percentage of WT activity. Data are mean ± S.D. (n=3 biological replicates, each with n=3-4 technical replicates; ***p<0.001 by one-way ANOVA). (B) Left, Blue native (BN)-PAGE immunoblot analysis of respiratory complexes in mitochondria from cells isolated at indicated growth times, detected with indicated antibodies. Right, SDS-PAGE immunoblot analysis of representative subunits of respiratory complexes IV (CcO; Cox1-3), III (bc_1; Rip1), II (SDH; Sdh2), and V (Atp2) and loading control (Porin) in mitochondria from these cells. (C) Mitochondrial DNA copy number of WT and *afg1*Δ strains grown in SC-glucose medium for the indicated number of days and analyzed by qPCR. The copy number was calculated as the nuclear (*ACT1* gene) to mitochondrial (*COX3* gene) DNA ratio and was set equal to one for WT samples. Data are mean values ± SD of 3 independent experiments, each with n=3 technical replicates. (D) Translation of the *COX1* ORF from the mitochondrial genome in young (12 hours post-inoculation) and aged (8 days post-inoculation) WT and *afg1*Δ cells, assessed by deleting *AFG1* in the *cox1*Δ*::ARG8* genetic reporter strain depicted schematically. Cells were cultured in SC-glucose medium supplemented with low amounts (4 mg/L) of arginine for the indicated periods of time and spotted onto SC-glucose (SCD) plates with (+Arg) or without (-Arg) arginine as well as on yeast extract-peptone-glycerol/lactate (YPGL) plates. The *arg4*Δ mutant served as a control. Plates were incubated for 3 (SCD plates) or 4 (YPGL plates) days at 28°C before photography. UTR, untranslated region.

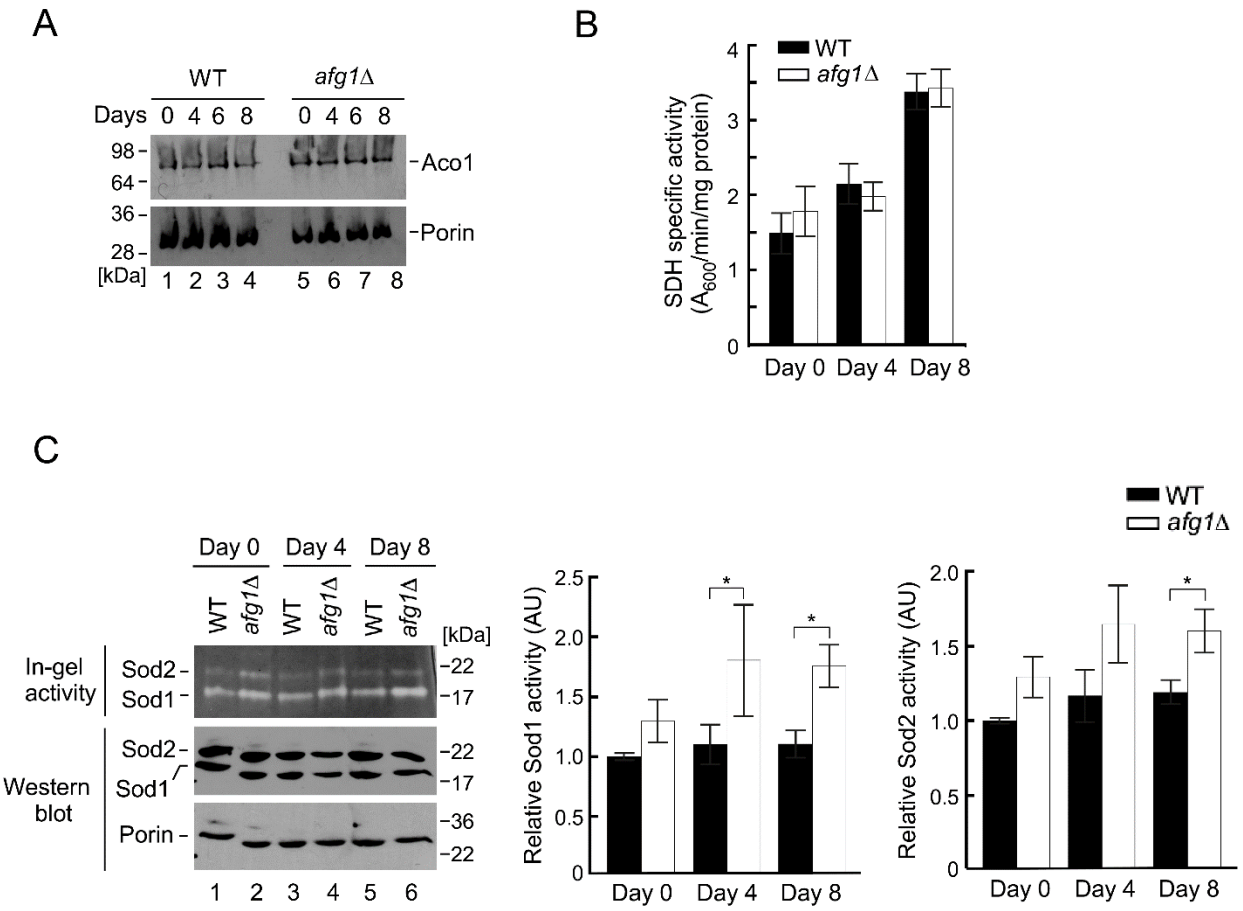

Figure S3. Loss of Afg1 does not impair aconitase steady-state levels or succinate dehydrogenase activity, while superoxide dismutase activity is elevated in aged cells lacking Afg1. (A) SDS-PAGE immunoblot analysis of the steady-state levels of aconitase (Aco1) and porin (loading control) in mitochondria described in Figure 3B. (B) Succinate dehydrogenase (SDH) enzymatic activity in mitochondria isolated from log-phase and 4- and 8-day-old WT and *afg1*Δ cells. Data are mean values ± SD of 3 independent experiments, each with n=3 technical replicates. (C) In-gel analysis of superoxide dismutase activity following native electrophoresis and assessment of steady-state levels of Sod1, Sod2, and porin following SDS-PAGE in the mitochondria described in Figure 3B. Quantitation of Sod1 and Sod2 in-gel staining signals is mean ± SD of 3 independent experiments, each with n=3 technical replicates; *p<0.05 by *t*-test.

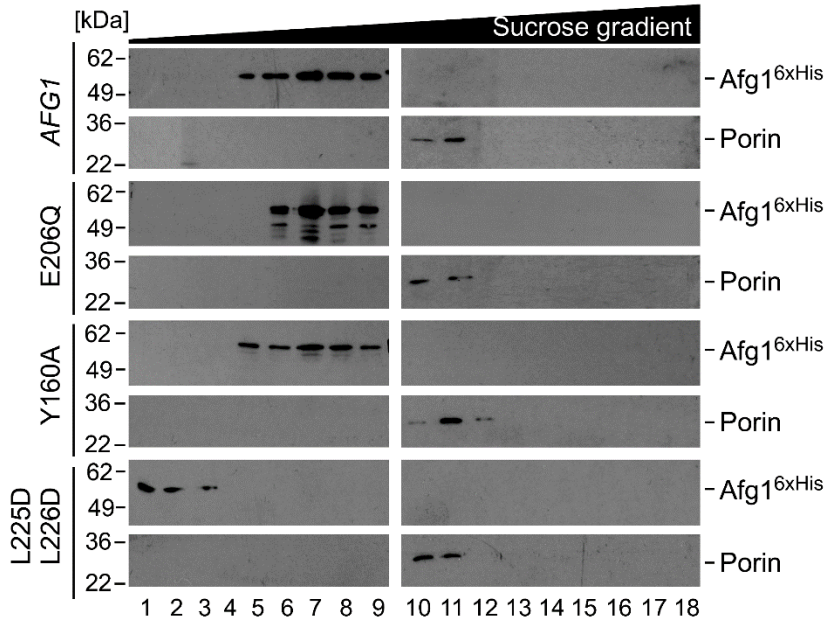

Figure S4. E206Q and Y160A variants of Afg1 are able to oligomerize. High-velocity fractionation of mitochondrial proteins from *afg1*Δ cells expressing Afg1-6xHis or its E206Q, Y160A, or L225D L226D variants solubilized with 1% digitonin. Following centrifugation on continuous sucrose density gradients (12-50%), gradient fractions were collected and analyzed by SDS-PAGE for distribution of Afg1 oligomers using anti-His antibody. The migration pattern of the 440-kDa porin complex (visualized with anti-porin antibody) was used for size comparison.

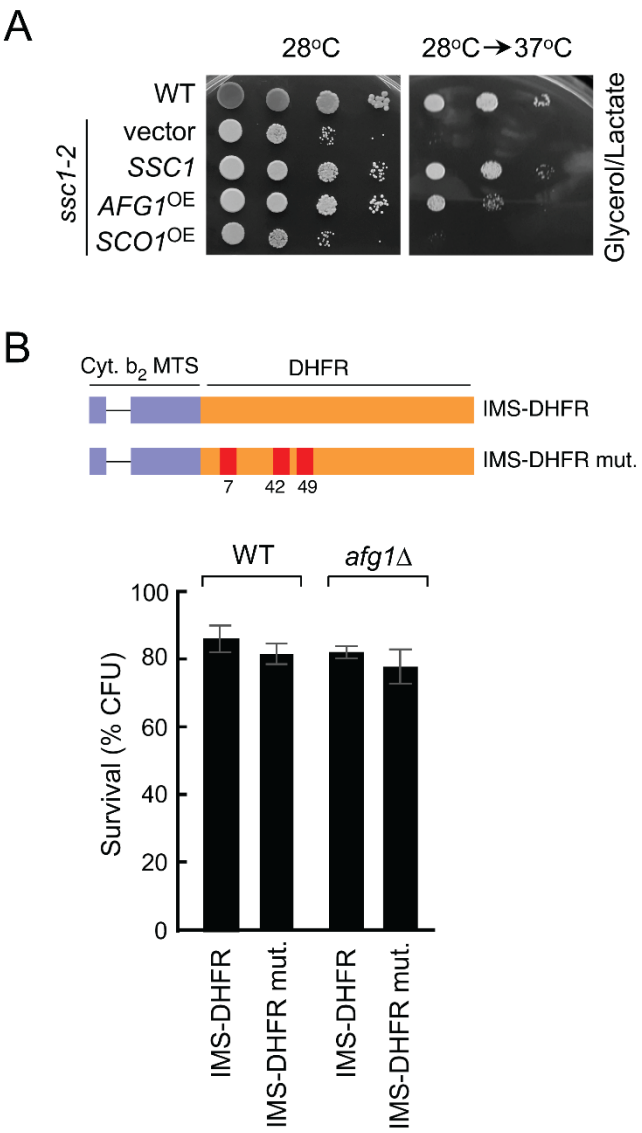

Figure S5. Afg1 over-expression partially compensates for the *ssc1-2* mutation, and a misfolding-prone protein targeted to the IMS in *afg1*Δ does not induce the growth defect observed for the matrix-targeted version. (A) Respiratory growth of WT and *ssc1-2* cells expressing vector control or *SSC1* or overexpressing *AFG1* or *SCO1* (negative control). Cells were handled as described in Figure 1A. (B) Top, schematic depiction of IMS-targeted DHFR chimeric protein consisting of the mitochondrial targeting/sorting moiety of yeast cytochrome b_2 (Cyt. b_2) fused to wild type (IMS-DHFR) or the misfolding-prone C7A, S42C, N49C variant of mouse DHFR (IMS-DHFR mut.). Bottom, colony viability of the indicated WT and *afg1*Δ transformants, assessed as described in Figure 5E. Data are mean values ± SD of 3 biological replicates, each with n=3 technical replicates.

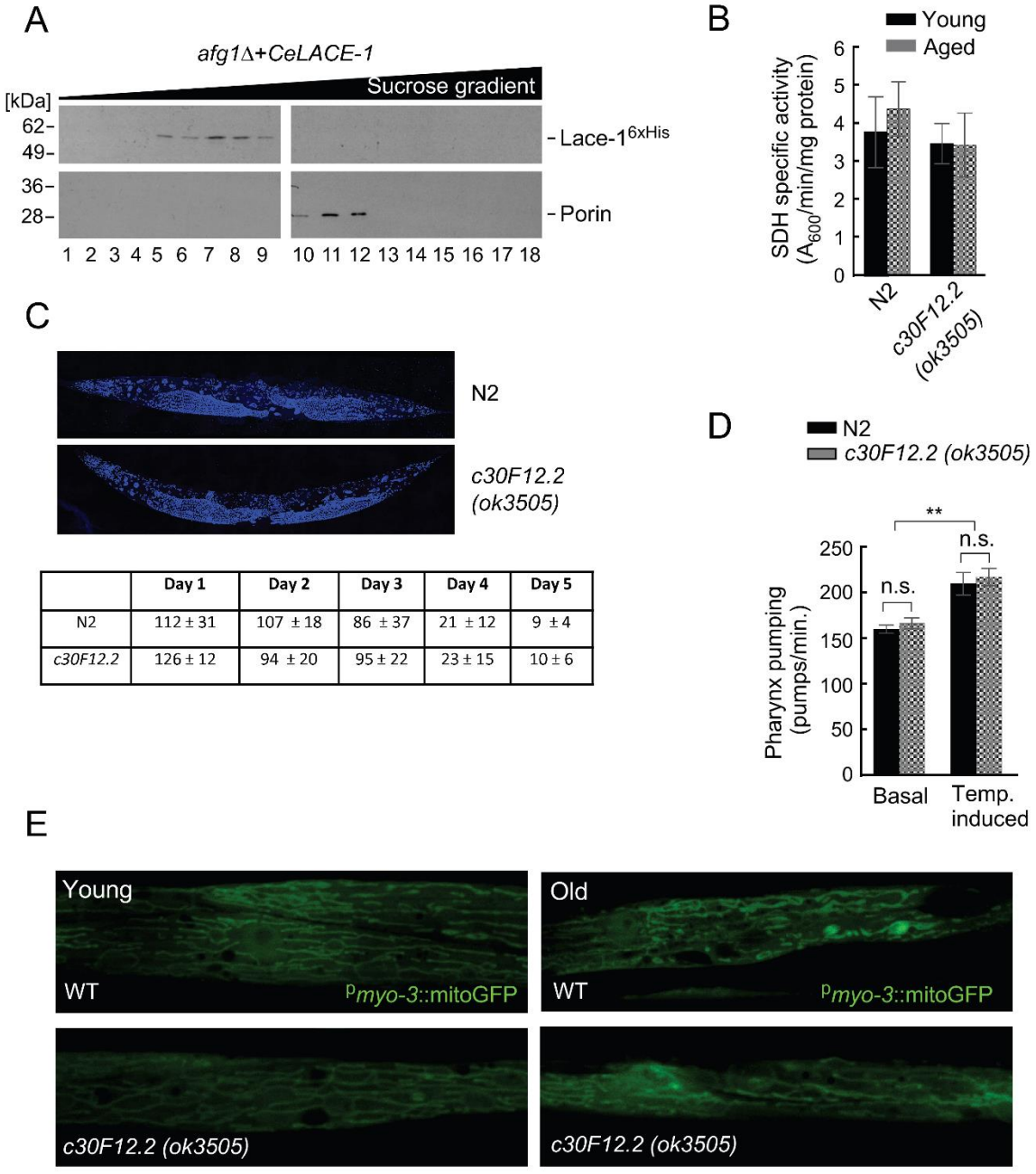

	Day 1	Day 2	Day 3	Day 4	Day 5
N2	112 ± 31	107 ± 18	86 ± 37	21 ± 12	9 ± 4
c30F12.2	126 ± 12	94 ± 20	95 ± 22	23 ± 15	10 ± 6

Figure S6. LACE-1 forms complexes similar to Afg1; worms lacking LACE-1 exhibit normal SDH activity, normal developmental phenotypes, normal basal and temperature-induced pharyngeal pumping rates, and normal muscle tissue mitochondrial networks.

(A) Density gradient fractionation of digitonin-solubilized mitochondria from yeast *afg1*Δ cells expressing C-terminally 6xHis-tagged *C. elegans* LACE-1 (*CeLACE-1*). The lysates were handled and analyzed as in Figure S4. (B) Enzymatic activity of succinate dehydrogenase in

mitochondria isolated from 1-day-old (young) and 5-day-old (aged) N2 and *c30F12.2(ok3505)* worms. Data are mean values ± SD (n=3 biological replicates with 3 animals per group). (C) Top, confocal micrographs (projected Z-sections) showing DAPI-stained N2 and *c30F12.2(ok3505)* animals. Bottom, average brood size of N2 animals and *c30F12.2(ok3505)* animals over 5 days. (D) Frequency of basal and temperature-induced pharynx movement (pumping) per minute in age-matched N2 and *c30F12.2(ok3505)* animals at day 1; n=3 with 10 animals per group. Data are mean values ± S.E.M.; n.s., not significant, **p<0.01 by *t*-test. (E) Representative fluorescence images of body wall muscle in age-matched WT and *c30F12.2(ok3505)* animals expressing ^{P}*myo-3::mitoGFP* mitochondria-targeted reporter at day 1 (young) and day 5 (old).

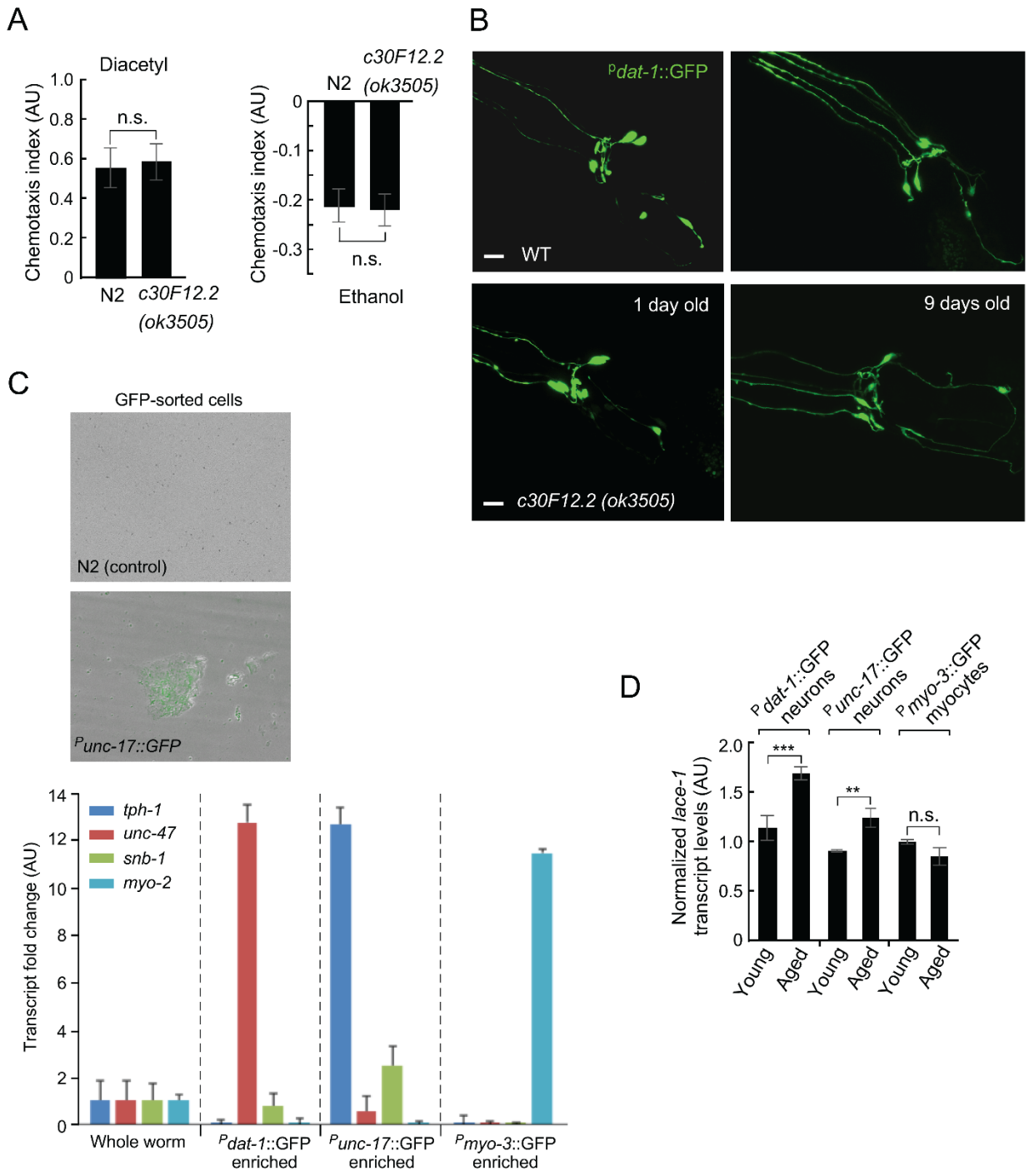

Figure S7. Worms lacking LACE-1 exhibit normal chemosensing and normal dopaminergic neurons; qPCR validates cell type following the isolation of GFP-sorted cells; worms exhibit increased expression of *lace-1* in neurons but not myocytes with aging. (A) Chemotaxis index of N2 and *c30F12.2(ok3505)* animals at Day 1. Worm responses

were tested for both attractive (diacetyl) and repulsive (ethanol) odorants; n=3 with 20 animals per group. Data are mean values ± S.E.M.; n.s., not significant by *t*-test. (B) Representative fluorescence images of dopaminergic neurons in 1-day-old (left) and 9-day-old (right) adult WT and *c30F12.2(ok3505)* animals expressing ^{P}*dat-1::*GFP reporter. (C) qPCR analysis of transcripts for the genes *tph-1*, *unc-47*, and *snb-1* (markers for neurons), and *myo-2* (marker for myocytes) and epifluorescent microscopy images showing the presence of GFP in the isolated cells. Image shows a single focal plane. (D) Transcript levels of *lace-1* in dopaminergic ^{P}*dat-1::GFP* neurons, cholinergic ^{P}*unc-17::GFP* neurons, and ^{P}*myo-3::GFP* myocytes isolated from relevant 1-day-old (young) and 5-day-old (aged) WT transgenic animals. Data are mean values ± SD (n=4 biological replicates with 4 animals per group; n.s., not significant, **p<0.01, ***p<0.001 by *t*-test).

Table S1. Yeast strains used in this study

Strain	Genotype	Reference/Source
W303-1B	*MATα ade2-1 can1-100 his3-11, 15 leu2-3, 112 trp1-1 ura3-1*	ATCC
W303-1B *afg1* Δ	*MATα ade2-1 can1-100 his3-11, 15 leu2-3, 112 trp1-1 ura3-1 afg1Δ::URA3MX*	This Study
W303-1B *oma1* Δ	*MATα ade2-1 can1-100 his3-11, 15 leu2-3, 112 trp1-1 ura3-1oma1Δ::HIS3MX6MX*	Bohovych et al., 2014
afg 1Δ *oma1* Δ	*MATα ade2-1 can1-100 his3-11, 15 leu2-3, 112 trp1-1 ura3-1 afg1Δ oma1Δ::URA3MX*	This Study
W303-1B *yta1* 0Δ	*MATα ade2-1 can1-100 his3-11, 15 leu2-3, 112 trp1-1 ura3-1 yta10Δ::HIS3MX6*	B. Meunier
yta10Δ oma1Δ	*MATα ade2-1 his3-1,15 leu2-3,112 trp1-1 ura3-1 yta10Δ::HIS3MX6 oma1Δ::TRP1*	This study
MB3 (*tim23-2*)	MATα ade2-101 his3-Δ200 leu2-Δ1 lys2-801 ura3::LYS2 tim23-2	N. Pfanner
cox1 Δ::ARG8	*MATα lys2 leu2-3, 112 arg8::hisG, ura3-52 [cox1Δ::ARG8m]*	Perez-Martinez et al., 2003
cox1 Δ::ARG8 *afg1* Δ	*MATα lys2 leu2-3, 112 arg8::hisG, ura3-52 [cox1Δ::ARG8m] afg1::URA3MX*	This study
DTY 833 (*arg4Δ)*	*MATa ade1Δ arg4Δ aro2Δ his7Δ lys5Δ ura2Δ*	D. Winge
MB4-1b *(sod2Δ)*	*MATa leu2-3,112 trp1-1 can1-100 ura3-1 ade2-1 his3-11,15 sod2Δ::KanMX*	A. Barrientos
afg 1Δ *sod2* Δ	*MATα ade2-1 can1-100 his3-11, 15 leu2-3, 112 trp1-1 ura3-1 afg1ΔSod2Δ::URA3MX*	This Study
PK81 (Ssc1-2)	*MATα his4-713 lys2 ura3-52 Δtrp1 leu2-3,112 ssc1-2::LEU2*	A. Barrientos
AFG1::6His	*MATα ade2-1 can1-100 his3-11, 15 leu2-3, 112 trp1-1 ura3-1 AFG1-His6::URA3MX*	This Study
AFG1::6His afg1Δ	*MATα ade2-1 can1-100 his3-11, 15 leu2-3, 112 trp1-1 ura3-1 AFG1-His6::URA3MX afg1Δ*	This Study
AFG1::6His yta10Δ oma1Δ	*MATa ade2-1 his3-1,15 leu2-3,112 trp1-1 ura3-1 AFG1-His6::URA3MX yta10Δ::HIS3MX6 oma1Δ::TRP1*	This study
AFG1::6His PK81	*MATα his4-713 lys2 ura3-52 Δtrp1 leu2-3,112 ssc1-2::LEU2 AFG1-His6::URA3MX*	This Study
SSC1::6His PK81	*MATα his4-713 lys2 ura3-52 Δtrp1 leu2-3,112 ssc1-2::LEU2 SSC1-His6::URA3MX*	This Study
SCO1::HA PK81	*MATα his4-713 lys2 ura3-52 Δtrp1 leu2-3,112 ssc1-2::LEU2 SCO1-HA::HIS3*	This Study